

# The Association of Large-Scale Climate Variability and Teleconnections on Wind Energy Resource over Europe and its Intermittency

Pascal Kriesche and Adam Schlosser



Report No. 250  
September 2013

The MIT Joint Program on the Science and Policy of Global Change is an organization for research, independent policy analysis, and public education in global environmental change. It seeks to provide leadership in understanding scientific, economic, and ecological aspects of this difficult issue, and combining them into policy assessments that serve the needs of ongoing national and international discussions. To this end, the Program brings together an interdisciplinary group from two established research centers at MIT: the Center for Global Change Science (CGCS) and the Center for Energy and Environmental Policy Research (CEEPR). These two centers bridge many key areas of the needed intellectual work, and additional essential areas are covered by other MIT departments, by collaboration with the Ecosystems Center of the Marine Biology Laboratory (MBL) at Woods Hole, and by short- and long-term visitors to the Program. The Program involves sponsorship and active participation by industry, government, and non-profit organizations.


To inform processes of policy development and implementation, climate change research needs to focus on improving the prediction of those variables that are most relevant to economic, social, and environmental effects. In turn, the greenhouse gas and atmospheric aerosol assumptions underlying climate analysis need to be related to the economic, technological, and political forces that drive emissions, and to the results of international agreements and mitigation. Further, assessments of possible societal and ecosystem impacts, and analysis of mitigation strategies, need to be based on realistic evaluation of the uncertainties of climate science.

This report is one of a series intended to communicate research results and improve public understanding of climate issues, thereby contributing to informed debate about the climate issue, the uncertainties, and the economic and social implications of policy alternatives. Titles in the Report Series to date are listed on the inside back cover.

Ronald G. Prinn and John M. Reilly  
*Program Co-Directors*

For more information, please contact the Joint Program Office

Postal Address: Joint Program on the Science and Policy of Global Change  
77 Massachusetts Avenue  
MIT E19-411  
Cambridge MA 02139-4307 (USA)  
Location: 400 Main Street, Cambridge  
Building E19, Room 411  
Massachusetts Institute of Technology  
Access: Phone: +1.617. 253.7492  
Fax: +1.617.253.9845  
E-mail: [globalchange@mit.edu](mailto:globalchange@mit.edu)  
Web site: <http://globalchange.mit.edu/>

 Printed on recycled paper

# The Association of Large-Scale Climate Variability and Teleconnections on Wind Energy Resource over Europe and its Intermittency

Pascal Kriesche<sup>\*†</sup> and Adam Schlosser<sup>\*</sup>

## Abstract

*In times of increasing importance of wind power in the world's energy mix, this study focuses on a better understanding of the influences of large-scale climate variability on wind power resource over Europe. The impact of the North Atlantic Oscillation (NAO), the Arctic Oscillation (AO), the El Niño Southern Oscillation (ENSO) and the Atlantic Multidecadal Oscillation (AMO) are investigated in terms of their correlation with wind power density (WPD) at 80 m hub height. These WPDs are calculated based on the MERRA Reanalysis data set covering 31 years of measurements. Not surprisingly, AO and NAO are highly correlated with the time series of WPD. This correlation can also be found in the first principal component of a Principal Component Analysis (PCA) of WPD over Europe explaining 14% of the overall variation. Further, cross-correlation analyses indicates the strongest associated variations are achieved with AO/NAO leading WPD by at most one day. Furthermore, the impact of high and low phases of the respective oscillations has been assessed to provide a more comprehensive illustration. The fraction of WPD for high and low AO/NAO increases considerably for northern Europe, whereas the opposite pattern can be observed for southern Europe. Similar results are obtained by calculating the energy output of three hypothetical wind turbines for every grid point over Europe. Thus, we identified a high interconnection potential between wind farms in order to reduce intermittency, one of the primary challenges in wind power generation. In addition, we observe significant correlations between WPD and AMO.*

## Contents

1. INTRODUCTION.....	2
2. BACKGROUND .....	2
2.1 Large-Scale Climate Variability and Teleconnections.....	3
2.2 Previous Work .....	6
3. DATA AND METHODOLOGY .....	8
3.1 Merra Data Set .....	8
3.2 Wind Power Density Computations .....	9
3.3 Wind Power Output Estimation.....	11
4. RESULTS AND DISCUSSION.....	13
4.1 Wind Power Distribution and Importance of Median and Mean Values .....	13
4.2 Principal Component Analysis over Europe.....	15
4.3 Influence of NAO/AO Indices on Wind Power Density.....	20
4.4 Explanation of the Impact of AO/NAO .....	30
4.5 Influence of the Atlantic Multidecadal Oscillation on Wind Power Density .....	32
4.6 Influence of the El Niño Southern Oscillation on Wind Power Density .....	34
5. CONCLUSIONS .....	34
6. REFERENCES .....	37
7. APPENDIX.....	41
7.1 Acronyms .....	41
7.2 Determination of Statistical Significance.....	42

---

<sup>\*</sup>Joint Program on the Science and Policy of Global Change, Massachusetts Institute of Technology, Cambridge, Massachusetts, USA.

<sup>†</sup>Corresponding author (email: kriesche@MIT.EDU).

## **1. INTRODUCTION**

The European wind industry is growing rapidly. Installed capacity has increased from around 13 GW in 2000 to more than 100 GW in 2012, meeting the power needs of 57 million households. That corresponds to 7% of Europe's electricity demand and to the output of 39 nuclear power plants (EWEA 2013). This positive trend will likely continue to increase in the next decade given that the European Union agreed that 20% of the total final energy consumption should come from renewables by 2020. Of course, wind energy already represents more than a fourth of all new EU power capacity installed in the last year and is one of the most promising energy resources to fulfill this ambitious objective. Given these great political conditions, the high potential of wind power and the fact that the technology itself is one of the most mature, it should be of primary importance to better understand the variability of the resource, and to provide solutions to lower its intermittency, as well as to balance its variability. Indeed, one of the biggest challenges for power companies is the ability to provide electricity on demand. As soon as wind resource fails, other sources must be available to compensate the shortage. Whereas diurnal and seasonal variability of wind is quite well known, and wind speed can be forecasted days in advance (e.g., Watson et al. 1994; Landberg et al. 2003; Torres et al. 2005), only a few studies have been conducted on the influences of teleconnections or large-scale climate variability on wind conditions over Europe. Nevertheless, teleconnections are of increasing scientific interest as can be seen in the ever-growing number of articles published during the last two decades. Besides, Europe has one of the most variable climates of any land area in the northern hemisphere (Woollings 2010). It is strongly affected by several processes, which are only poorly represented in current models. Understanding year-to-year variability of wind power density will further help to better anticipate potential energy output and consequently to judge more accurately the economical feasibility of commercial wind farm projects. Thus, the purpose of the present study will be to evaluate the association of teleconnections such as the Atlantic Oscillation (AO) and the North Atlantic Oscillation (NAO), and large-scale climate variability, in the case of the Atlantic Multidecadal Oscillation (AMO) on wind power density over Europe. In addition, the impact of the El Niño Southern Oscillation (ENSO) is also investigated. The objective will be to provide a comprehensive way to understand and to quantify these influences. For instance, in addition to Principal Component Analysis and correlation studies, wind energy output will be estimated for all of Europe using three different model wind turbines. Furthermore, solutions to reduce intermittency will be proposed.

## **2. BACKGROUND**

Before presenting the methodology applied for the present study and discussing its results, it is important to recall some definitions and to have a closer look at what has already been done in previous studies.

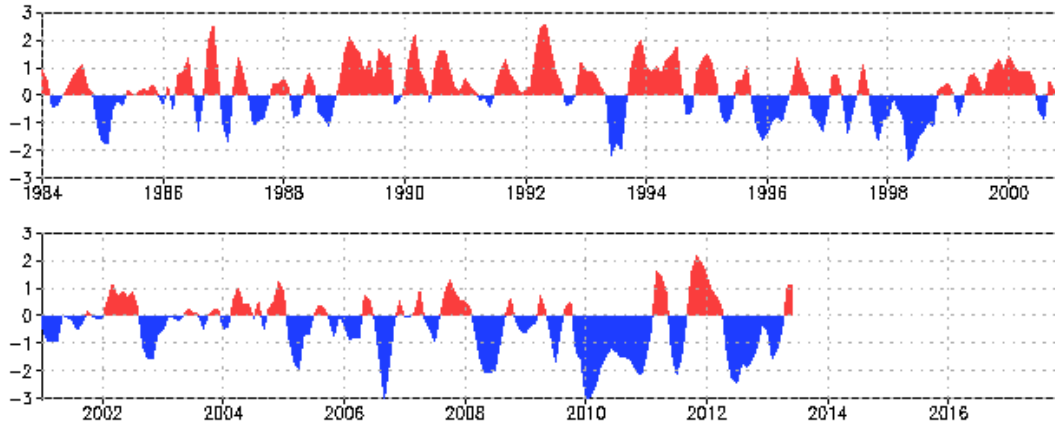


**Figure 1.** NAO index using a 3-month running mean  
 (source: NOAA, [http://www.cpc.ncep.noaa.gov/products/precip/CWlink/pna/month\\_ao\\_index.shtml](http://www.cpc.ncep.noaa.gov/products/precip/CWlink/pna/month_ao_index.shtml)).

## 2.1 Large-Scale Climate Variability and Teleconnections

A "teleconnection pattern" in a meteorological field may be defined as a spatial structure with two or more distinct and strongly coupled centers of action according to Deser (2000). The Oscillations presented in the following will be studied in terms of their association with wind power resource over Europe. All the teleconnection indices used are available on the NOAA website.

### *North Atlantic Oscillation*

The North Atlantic Oscillation has been subject of much interest in the last decades (e.g., Wallace and Gutzler 1981; Hurrell 1995). It is the dominant, large-scale extra-tropical teleconnection pattern in the Atlantic sector according to Visbeck et al. (1998). It consists of a north-south dipole of anomalies, with one center located over Greenland and the other center of opposite sign spanning the central latitudes of the North Atlantic between 35°N and 40°N. Its phase is indicated by the NAO index measuring the normalized pressure difference between a station in the Azores, for instance in Portugal, and one in Iceland. In other words, the NAO represents a large-scale meridional oscillation of atmospheric mass between the subtropical anticyclone near the Azores and the subpolar low-pressure system near Iceland (van Loon and Rogers 1978). For our studies we used a daily NAO index. **Figure 1** shows the variation of this index over the last 29 years smoothed using a 3-month running mean.

As we can see, it is characterized by interannual and interseasonal variability. It is not unusual to observe periods of several months of both positive and negative phases of the teleconnection. According to Hurrell (1995) the wintertime NAO also shows significant multidecadal variability.

Atkinson et al. (2006) found that NAO has a particularly dominant effect on the climate during winter months. As stated by NOAA the positive phase of the NAO reflects below-normal heights and pressure across the high latitudes of the North Atlantic and above-normal heights and pres-

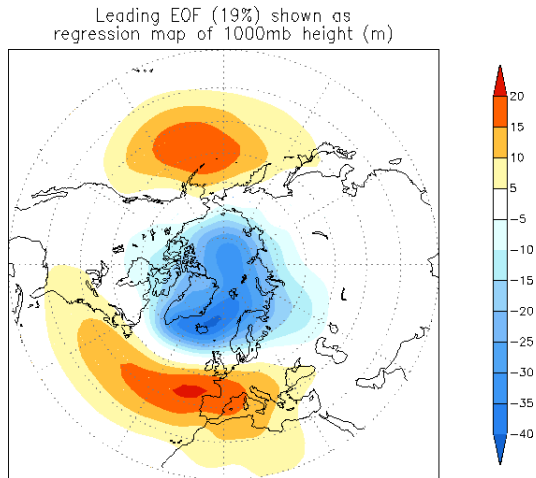


**Figure 2.** The AO (source: NOAA).

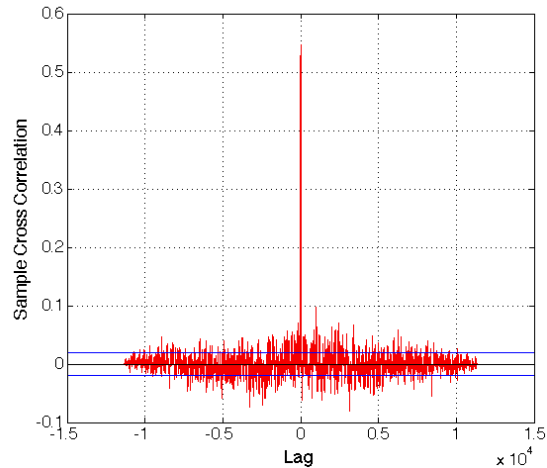


**Figure 3.** Correlation sequence between AO and NAO.

sure over the central North Atlantic, the eastern United States and western Europe. An opposite pattern of heights and pressure anomalies over these regions is observed during the negative phase. Both phases of the NAO are associated with the strength and position of maximum surface westerlies across the Atlantic and into Europe, van Loon and Rogers (1978). These are prevailing winds in the middle latitudes, between  $30^{\circ}$  N and  $60^{\circ}$  N latitudes and thus blowing over Europe. Thus, a positive index is associated with windier, warmer and wetter winters in Northern Europe and a negative one with less windy, colder and drier winters.

### *Arctic Oscillation*

Following the earlier studies of Lorenz (1950) and Kutzbach (1970), Thompson and Wallace (1998) introduced the nomenclature "Arctic Oscillation" (AO) to describe the leading Empirical Orthogonal Function (EOF) of monthly Sea Level Pressure (SLP) anomalies during winter pole wards of  $20^{\circ}$  N (see **Figure 2**). EOFs are the eigenvectors of the covariance matrix. We obtain them by calculating the covariances of time series at different spatial points (e.g., Jolliffe 1986). EOFs are best in explaining the maximum total variance with any specified number of spatial patterns. An increase in the AO implies a strengthening of the polar jet over northwestern Europe and of the subtropical jet in the same sector. Because of the overlap of the NAO and AO patterns in the Atlantic sector, the time series of the two patterns are highly correlated according to Ambaum et al. (2001). To confirm that, we calculated the correlation between these two daily indices for a time period of 31 years and obtained a correlation coefficient of 0.54 at no lag between both time series (see **Figure 3**). Nevertheless, Thompson and Wallace emphasized the AO's higher degree of zonal symmetry and suggested that it should be regarded as the more fundamental structure. In their view, the NAO is largely an "historical accident" dictated by station data availability.

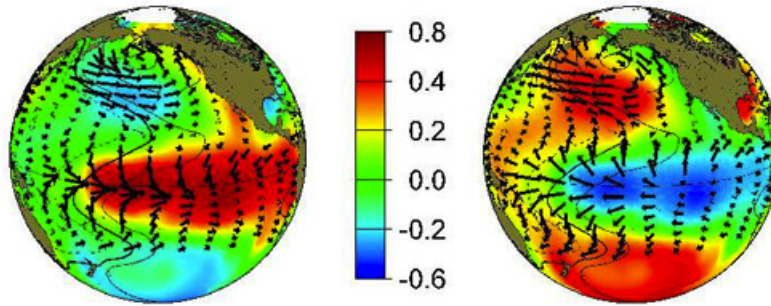


**Figure 4.** El Niño (left) and La Niña (right). Red and blue areas indicate temperature anomalies. Wind stress directions and magnitudes are indicated by vectors.  
 (source: [http://ffden-2.phys.uaf.edu/645fall2003\\_web.dir/jason\\_amundson/enso.htm](http://ffden-2.phys.uaf.edu/645fall2003_web.dir/jason_amundson/enso.htm)).

According to Ambaum the NAO pattern can be identified in a physically consistent way in PCA applied to various fields in the Euro-Atlantic region, but no such identification is found for the AO.

### *El Niño Southern Oscillation*

As the globally dominating mode of interannual climate variability El Niño–Southern Oscillation (ENSO) affects vast regions of the tropics, the Pacific, and the Indian Ocean as well as the surrounding landmasses (Brönnimann 2007). According to NOAA, El Niño is characterized by unusually warm temperatures and La Niña by unusually cool temperatures in the equatorial Pacific (see **Figure 4**). ENSO phases occur every few years and last for about a year. They can cause severe droughts in one part of the world and devastating floods in other parts (Philander 1989).

Previous studies of ENSO teleconnections mostly stated a relatively small effect in Europe (Ropelewski and Halpert 1987). Nevertheless, Fraedrich and Müller (1992) found that there is a consistent ENSO signal in European climate influencing temperatures and precipitations.

### *Atlantic Multidecadal Oscillation*

Named by Kerr (2000) the Atlantic Multidecadal Oscillation (AMO) can be defined as the area averaged Sea Surface Temperature (SST) anomaly over the Atlantic (0-70°N) minus the global mean SST anomaly. It has a period of 65-70 years (Schlesinger and Ramankutty 1994).

There are several examples of regional multidecadal climate variability related to AMO, for instance, European summer climate, especially precipitation and temperatures (Sutton and Hodson 2005). Further AMO is thought to be driven by the ocean’s thermohaline circulation that is a part of the large-scale ocean circulation driven by global density gradients created by heat and fresh water fluxes. It may be predictable several decades in advance (Knight et al. 2005). A positive AMO anomaly results in decreased sea level pressure and increased rainfall in northwestern Europe. Further, AMO modulates the Atlantic tropical cyclone activity (Goldenberg et al.

2001). The exact relationship between the low frequency SST modes, higher frequency atmospheric modes (AO/NAO) and terrestrial climates must still be resolved (Gray et al. 2004). Kushnir (1994) found a mutual relationship between interannual fluctuations of SST and surface wind conditions suggesting that the former are maintained by the latter through a local thermodynamic interaction.

## 2.2 Previous Work

Most of the studies on the impact of teleconnection over Europe, especially NAO, focus on variations in precipitation and temperature (e.g., van Loon and Rogers 1978 or Hurrell 1995). Some are looking at WS variations, whereas only a few consider wind power density (WPD) over Europe as for example Pryor et al. (2005) or Cosseron et al. (2013). The former aims to assess the historical variability of wind indices across different spatial scales and the degree to which robust projections of future wind energy density can be derived. The latter characterizes wind power resource over Europe and its intermittency by studying metrics such as availability and episode length or also Anti-coincidence and Null Anti-coincidence as defined by Gunturu and Schlosser (2012).

Regarding the association of NAO with WS, Hurrell et al. (2003), state that a change in NAO phase produces large changes in the mean WS and direction over the Atlantic and the intensity and number of storms. Pirazzoli et al. (2010) were then the first to relate changes in measured WS and directions in the northeastern Atlantic with NAO on a larger scale of latitudes between  $66^{\circ}\text{N}$  and  $44^{\circ}\text{N}$ , thus covering the west coast of northern Europe. They therefore used wind measurements, recorded since the 1950s, at twelve meteorological stations and divided them into three periods: 1950–75, 1976–92 and 1993–2008. Using monthly or seasonal means and restricting the data to the cold season from October to March, they observed important changes in time and latitude in the correlation with the NAO index. The highest correlation coefficients (about 0.7) were observed for the early time period between  $58^{\circ}\text{N}$  and Iceland, whereas low positive coefficients were reported more south. During the second period, characterized by a mostly increasing NAO index, positive correlation (up to 0.8) improves southwards as far as  $54^{\circ}\text{N}$  (Belmullet) with some improvement also at Shannon and Valentia, but it remains low or even negative near the French Atlantic coast. Finally in the latest period, correlation improved for all the stations south of  $54^{\circ}\text{N}$ , while it weakens more in the North. It is stated that the most significant for correlation with NAO is indeed the average WS for all directions. Therefore we will not consider the impact of NAO on wind direction in the present. It is concluded that correlation between wind and NAO increase for the northern stations and decrease for the southern ones in the case of a positive NAO index. For a negative NAO index the opposite occurs. This is mainly explained by the direction of local dominant winds at each station. For example, in the North, easterlies are



dominant since the main storm tracks pass within the 60–65°N belt, whereas more southern westerlies are dominant since these stations are just below the main storm tracks.

Atkinson et al. (2006) compared the NAO index with windiness indices from Germany, Denmark, Netherlands and the UK over a period from 1990 to 2005. Their goal was to discuss the use of NAO as proxy for WS in order to investigate a trend over the last 40 years. They obtain an average coefficient of determination  $R^2$  of 0.49 that is high enough to make conclusions on a long-term trend and to justify the qualitative but not quantitative use of these proxies.

A more recent study by Brayshaw et al. (2011) reveal some interesting results. They are the first and only to have investigated the influence of different NAO states on the power output of a hypothetical wind turbine model at two specific sites in the United Kingdom: the coastal airport of Stornoway (STO) on an island in northwestern Scotland and Great Dunfell (GDF), an exposed upland area in the central UK. Monthly WS records during the cold season at 10 m hub heights for time periods from 1969 to 2004 in the case of GDF and from 1957 to 2002 in the case of STO have been used. These are multiplied by a constant scaling factor in order to obtain the WSs at 80 m and categorized into three different NAO states: High (NAO index  $\geq 0.5$ ), medium ( $0.5 >$  NAO index  $> -0.5$ ), low (NAO index  $\leq -0.5$ ). It is noted that the choice of the scaling factor contains some arbitrariness. The resulting power outputs for each state are then calculated. A transition from low to high NAO results in a significant increase in the power output: 18.6% at STO and 11.3% at GDF. Furthermore, preliminary research for the mentioned study found strong impacts of NAO on WPD for another site close to GDF but at sea level next to the coast and much weaker impacts for London Heathrow located in Southeast England. We are going to extend and generalize their approach on a large scale in the present study.

Jerez et al. (2013) evaluate the impact of the NAO on the interannual variability of the main primary renewable energy resources in Portugal and Spain. Therefore a holistic assessment based on a 10 km-resolution climate simulation based on the regional model MM5 over the period from 1959 to 2007 has been done providing physically consistent data of the different fields involved. It is shown that a negative NAO phase enhances WS by 10–15%, and thereby wind power at typical wind turbines heights by around 30%. The cited study is still in press and thus highlights the high scientific interest in the present topic.

As presented above, apart from Jerez et al. (2013), all existing investigations regarding the impact of teleconnections on WSs have been conducted for a limited number of measurement stations. None has ever looked at the impact of teleconnection over a larger scale over all of Europe. Besides most of the studies provide qualitative results whereas a comprehensive quantitative measure of the impact of teleconnections is missing. Since the previous studies were averaging the used data over at least one-month periods there is no evidence about the lead/lag between teleconnection and WPD. Since the NAO is often considered as the most robust climate teleconnec-



**Figure 5.** The two considered geographical domains: core Europe (orange box) and wider Europe (blue box) (source: <https://maps.google.com/> ).

tion in the Northeastern Atlantic (Hurrell and Deser 2009), most studies focus on this teleconnection pattern. But, what about AO, AMO and ENSO? Furthermore, it would be much more accurate to study WPD than WS as it will be explained later. Finally, until present no study has proposed solutions to intermittency issues by teleconnection variations. All these open questions will serve as a motivation for our present study.

### 3. DATA AND METHODOLOGY

In this report we present results of our studies for two geographical domains (see **Figure 5**). A first one, referred to as “core Europe“, scans Europe from 34°N to 71.5°N latitudes and from 11°E to 41°W longitudes. It spreads from Portugal to the western end of Ukraine. A second one, referred to as “wider Europe“ considers a larger range of longitudes from 26°E to 42°W, and thus includes Iceland and the eastern Atlantic. Both domains also take into account offshore regions. If not stated differently we used the first domain by default as it concentrates on the areas over land and the coastal regions we are interested in and helps us to reduce capacity requirements for our calculations. The meaning of all the following acronyms can be found in the appendix of this report.

#### 3.1 Merra Data Set

Researchers often used measurements from airports or meteorological towers at different heights to extrapolate WSs to the wind turbine hub heights. For instance, Archer and Jacobson (2007) used the upper air measurements from rawinsondes and balloons at the nearest meteorological stations to extrapolate the WSs at 10 m to the hub height at 50 m or 80 m. Kiss and Janosi (2008) used the ECMWF’s ERA-40 reanalysis of eastward and northward winds at 10 m, that

covers a time period of 44 years in order to study wind field statistics over Europe. Larsen and Mann (2009) also used reanalysis data from NCEP/NCAR to estimate the geostrophic wind and extrapolated it to 10 m heights. Similarly, many researchers used a power or logarithmic law assuming roughness length and friction velocity in the boundary layer that did not vary with seasons, terrain and stability of the atmosphere.

To counter these limitations, we decided to use the Modern Era Retrospective-Analysis for Research and Applications (MERRA) data to reconstruct the wind field at 80 m. It is a reconstruction of the atmospheric state by assimilating observational data from different platforms into a global model (Rienecker et al. 2011). The data assimilation included conventional data from many sources as well as data from several trains of satellites. Conducted at the NASA Center for Climate Simulation, MERRA aims to provide a more accurate data set using the comprehensive suite of satellite-based information for climate and atmospheric research. The present data set has been constructed with GEOS-5 ADAS (version 5.2.0). The system consists of the GEOS-5 model and the GSI analysis. GSI has been developed by GMAO and NOAA's National Centers for Environmental Prediction jointly. The MERRA Data Set has a spatial resolution of  $1/2^\circ$  (lat) x  $2/3^\circ$  (long) and a time resolution of an hour. Since jumps in intensity within one hour are averaged, variability on time scales below one hour cannot be studied with this data set. The data spans a period over 31 years from 12:30 AM on January 1, 1979 to 11:30 PM on December 31, 2009. Thus, the data set allows us to look at the wind variations over several scales up to the decadal scale. In our studies we are considering three types of data sets:

- Whole data: All the available hourly data
- Cold season: A restriction of that data on the months from November to March
- Winter season: A restriction of the whole data on the winter months from January to March

### 3.2 Wind Power Density Computations

About 20 years ago, the usual wind turbine height was 50 m. The advancement of technology allowed raising the hub height of turbines to 80 m and higher. Since 80 m hub heights are the most common today we will focus on these heights in our studies. As we are considering power generation, it is more accurate to study WPD rather than WS. Indeed, the former takes into account air density, a crucial feature to assess potential power that could be harvested. The wind power density at each time step can be estimated by the formula:

$$WPD = \frac{1}{2}\rho(W S)^3 \tag{1}$$

where  $\rho$  represents the air density. We assume that the air density does not differ considerably at these heights through the well-mixed boundary layer. Thus, we use the air density at the center

of the lowest model layer  $\rho$ . MERRA already provides WSs but they do not take the roughness of the boundary layer into account given that they are computed from pressure gradients. Thus, we prefer to calculate the necessary WSs at 80 m hub height on our own using similarity theory in boundary layer dynamics. According to Stull (1988), it is based on the observation that for a number of boundary layer situations, the knowledge of the governing physics is not sufficient to derive laws from first principles. Nevertheless, boundary layer observations frequently show consistent and repeatable characteristics, suggesting that empirical relationships for the variables of interest can be developed. Similarity theory provides a way to organize and group the variables to our maximum advantage and in turn provides guidelines on how to design experiments to obtain the most information. It is based on the organization of variables into dimensionless groups through a four-step process. The result of it is an empirical equation or a set of curves showing the same shape. Since the curves look self similar it has been called similarity theory.

The atmospheric boundary layer is mainly controlled by the surface heat flux and the aerodynamic roughness length of the surface,  $z_0$ . It is defined as the height where the WS theoretically becomes zero. It is called aerodynamic since the only true determination of this parameter is from measurements of the WSs. Besides, if the individual roughness elements are packed very closely together, for instance in the case of a forest, then the top of those elements begins to act like a displaced surface. Hence a displacement distance,  $d$ , can be defined.

In addition, the maintenance of winds in the boundary layer depends on the stability of the atmosphere. The shear-stress in the boundary layer is estimated by the friction velocity  $u_*$ .

With these parameters, the WS at a height  $z$  in the boundary layer can be calculated using a logarithmical wind profile:

$$WS_z = \left(\frac{u_*}{\kappa}\right) \log \left[ \frac{(z-d)}{z_0} - \psi \right] \quad (2)$$

where  $\kappa$  is the von Karman constant.  $\psi$  is a function that depends on the stability of the boundary layer. For this study, the boundary layer is assumed to be neutrally stable, avoiding thus the additional  $\psi$  function. This assumption seems reasonable knowing that, at the high WSs at which wind power is harvested, the boundary layer has large wind shear making it approximately neutrally stable. Thus, for statically neutral conditions, we obtain:

$$WS_z = \left(\frac{u_*}{\kappa}\right) \log \left[ \frac{(z-d)}{z_0} \right] \quad (3)$$

$WS_z$  is well defined to be zero at  $z = d + z_0$ . As described above, our estimates take into account the effects of surface heat flux on the friction velocity, the time variation in displacement height and roughness length. As such, our estimates are more explicit and comprehensive.

**Table 1.** Characteristics of the three wind turbines used (VESTAS). WS in [m/s], height in [m] and swept area in [ $m^2$ ]

Turbine	Product name	Cut-in WS	Rated WS	Cut-out WS	Height	Swept area
Model 1	V100-2.0MW	3	12	20	80	7.854
Model 2	V90-3.0MW	3.5	15	25	80	6.362
Model 3	V112-3.3MW	3	13	25	84	9.852

Finally, we obtain for the at a height  $z$ :

$$WPD_z = \frac{1}{2}\rho \left[ \left( \frac{u_*}{\kappa} \right) \log \left[ \frac{(z-d)}{z_0} \right] \right]^3 \quad (4)$$

The MERRA data set provides us with all the necessary data for  $\rho$ ,  $u_x$ ,  $d$  and  $z_0$ . It is important to note that the data used and the methodology described above has already been used in previous studies, for instance in Gunturu and Schlosser (2012) and Cosseron et al. (2013).

### 3.3 Wind Power Output Estimation

The WPD can be used to estimate a theoretical upper bound for the wind power that can be harvested by a wind turbine characterized by an efficiency  $\eta_{eff}$  and sweeping an area  $A$  at a certain location by:

$$P_{tot,max} = \eta_{eff} \cdot A \cdot PWD \quad (5)$$

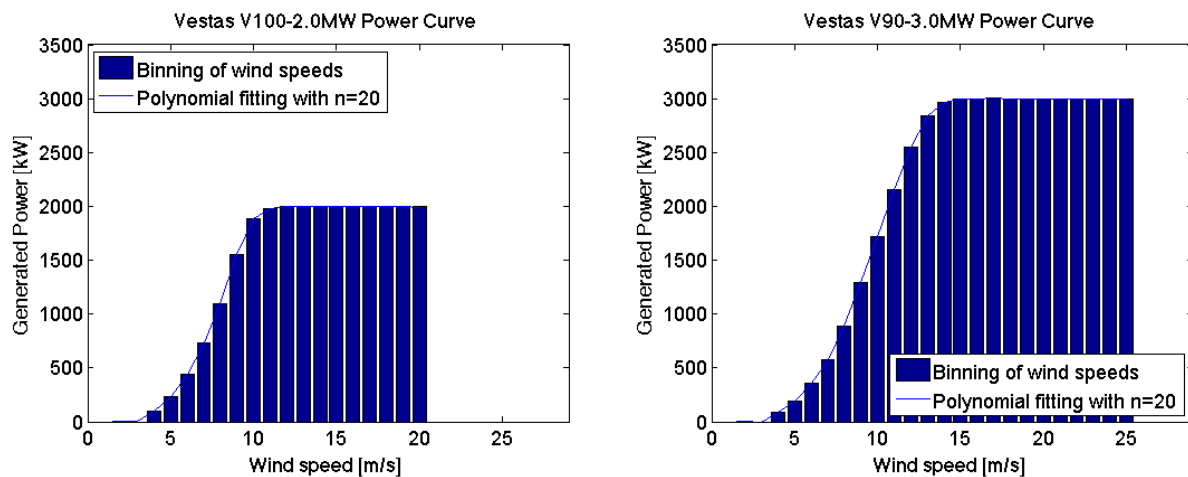
Unfortunately this metric does not take into account the technical features of the real wind turbine used. If we wish to calculate a more accurate estimate, for instance the energy output of a turbine, we need to consider the WS distribution at the one hand and a power curve of a specific model turbine on the other hand.

The power curve alone does not provide any valuable information about the energy that will be extracted in the end. For example, it could be that the WSs at a certain location are much too high or too low and thus they would be outside of the operable range of the turbine. In general, a power curve indicates the possible electrical power output at different WSs. It is characterized by the

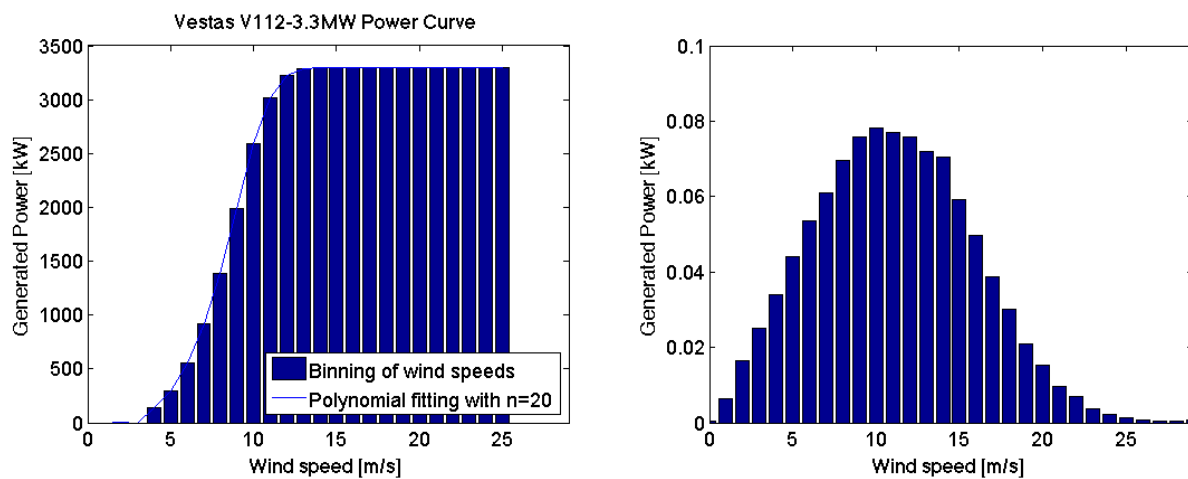
- Cut-in WS: lowest operable WS
- Rated WS: point where turbine starts operating at its maximum
- Cut-out WS: highest operable WS

For our studies we used three different wind model types from VESTAS (2013), largest wind turbines manufacturer in the world (Table 1).

Further technical details of the wind turbines used can be found in the VESTAS product brochures. We modeled the respective power curves using a polynomial fit of degree 20 as shown in **Figure 6**.



(a) Left: Power curve for Model 1; Right: Power curve for Model 2.



(b) Left: Power curve for Model 3; Right: PDF of WS in Munich (GER)

**Figure 6.** Power curves for the three different wind turbines chosen (VESTAS) and exemplary WS distribution.

As all wind turbines have hub heights around 80 m, we will use WS data at these heights. The air density will be assumed constant as suggested by VESTAS ( $\rho = 1.225 \frac{kg}{m^3}$ ). Model 2 corresponds exactly to the wind turbine used by Brayshaw et al. (2011) and has been chosen in order to compare their results with ours. In addition we also chose one of VESTAS latest releases (April 2013) as a model for a high performance wind turbine (Model 3) as well as a smaller one (Model 1). Model 3 has the great advantage that it can be used for both onshore and offshore installations. As we are going to calculate the generated power for every grid point over Europe, we preferred not to limit our analysis to a single wind turbine. In reality the wind turbines should be selected for every location separately according to the prevailing wind distribution.

Based on WS distribution and power curve we can calculate the generated energy by:

$$E = \int_0^{\infty} h(WS)P(WS) \quad (6)$$

where  $h(WS)$  represent the relative frequency of occurrence of a given WS and  $P(WS)$  the respective possible power output from the power curve. In order to reduce calculating time and memory we will reduce the integral to a sum over discrete values of the energies  $E_i$  :

$$E = \sum E_i = T \sum h_i P_i \quad (7)$$

where  $h_i = \frac{t_i}{T}$  is the relative frequency of occurrence of a bin of  $WS_i$  and  $t_i$  the part of the total time  $T$  over which we measured  $WS_i$ . As shown by the blue bins in the figures we discretized both power curve and WS PDF by using the same sample size  $h = 30$  and thus obtain  $P_i$ . The considerations above are taken from Gasch and Twele (2011).

Basically, we are interested in two metrics:

1. The total annual energy output in kWh (an example distribution of the annual energy output is shown for Munich in **Figure 7**).
2. The capacity factor (CF) defined as:

$$CF = \frac{\text{generated energy output}}{\text{maximum possible energy output}} \quad (8)$$

These metrics will be calculated for each grid point and for each wind turbine model.

## 4. RESULTS AND DISCUSSION

### 4.1 Wind Power Distribution and Importance of Median and Mean Values

Before we start going into the detail of the diverse impacts of teleconnections it is worth looking at the WPD distributions. Morrissey et al. (2010) suggest studying the WPD distribution

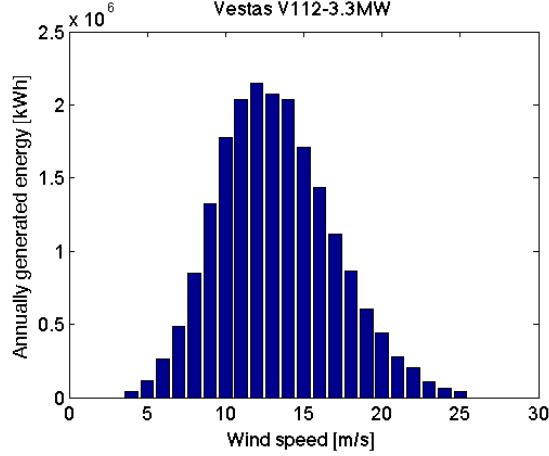


**Figure 7.** Annual energy output distribution using Model 3 for Munich (48.1°N, 11.6°E).

rather than the WS distribution when computing a WPD distribution. Small errors in the estimation of the WS probability function (PDF) can result in large errors in the WPD distribution curve since the cubic term in the WPD function amplifies the error. Jaramillo and Borja’s (2004) argue that it is not possible to generalize the two-parameter Weibull distribution:

$$f(WS) = \left(\frac{k}{c}\right) \left(\frac{WS}{c}\right)^{k-1} \exp\left[-\left(\frac{WS}{c}\right)^k\right] \quad (9)$$

where  $c$  is the scale and  $k$  the shape factor which is dimensionless, since it is not accurate to represent some wind regimes as shown in the case of La Ventosa in Mexico. Morrissey gives another extreme example of WS distribution for Boise city, Oklahoma, underlining that WS does not always have a Weibull-like distribution. Using the Weibull distribution for WS data underestimates the frequencies of lower WSs and overestimates those of the higher speeds, which results in an overestimation of the resource. Even though, the Weibull distribution remains the most widely distribution to model as accurately as possible WS distributions. Thus, it is relevant to be fully aware of the limits of this distribution in modeling actual WS.

**Figure 8** shows the WPD distribution for Munich (48.1°N, 11.6°E) as an example grid point. Given the long-tailed profile of the WPD distribution the mean value seems not to be a robust measure of the center of this distribution. The deviation of the mean from the actual center of this distribution is caused by the extreme value. Nevertheless, the median value seems to represent a central tendency. We will therefore consider the median to be a more relevant indicator of central tendency and a more appropriate metric to represent WPD especially in our studies that follow. Those considerations are important for anyone who wants to be able to estimate accurately the required backup or power produced by wind turbines at one location. Furthermore, Hennessey (1977) had shown that wind power studies based only on the total mean do not give an accurate picture of the wind power potential of a site and omit valuable information in terms of intermittency and variability.



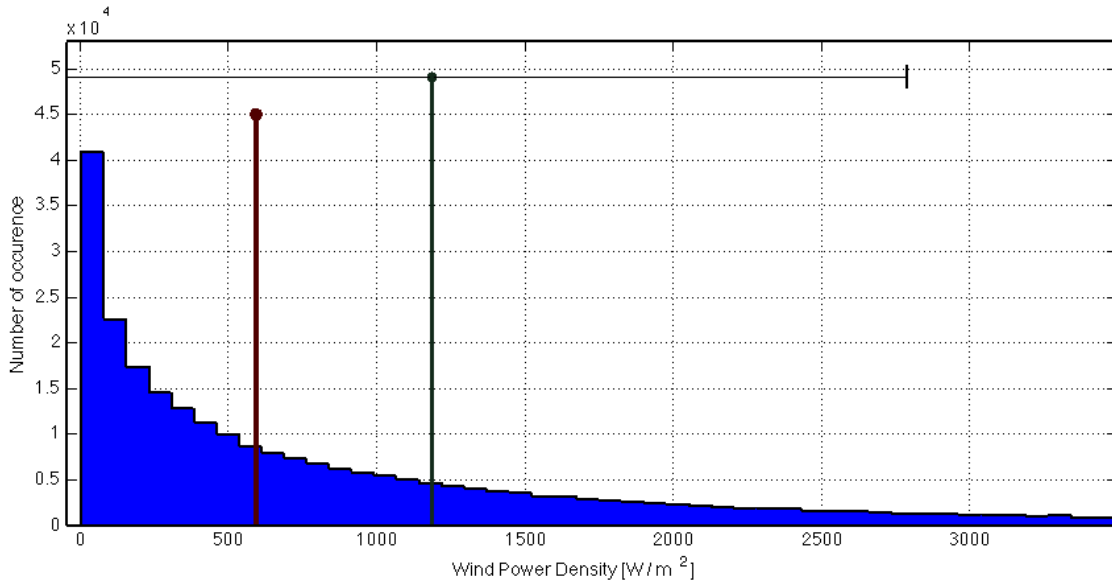


**Figure 8.** WPD distribution for Munich (GER) as an example. The median value of the distribution is plotted in red, the mean in black.

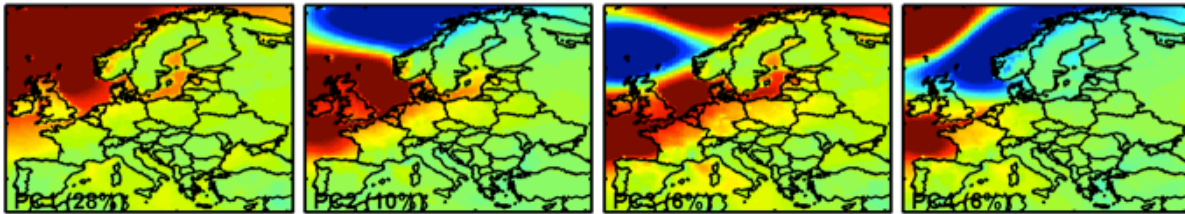


**Figure 9.** The first 4 PC coefficients from the PCA of hourly WPD whole data set over core Europe. The values in parentheses are the percentage of variance explained by that PC.

## 4.2 Principal Component Analysis over Europe

First, a PCA has been conducted on our WPD data over Europe in order to break down into independent variables the numerous influences on wind energy resource. Our aim will then be to associate some of the principal components with different teleconnection indices. This first overall approach will enable us to better understand our data set and will hopefully provide us useful hints about large-scale climate impacts which will be studied in a more detailed way in the following chapters.

### *Eigenvectors of the first principal components*

PCA reduces the dimensionality of a set of data into vectors of dominating variance, where the first Principal Component (PC) explains the most variance, the second explains the second-most, etc. **Figure 9** shows the coefficients, or eigenvectors, of the first four PCs of a PCA that has been run over the hourly whole data set for core Europe. The first PC explains 28% of the variance; the second explains 10%, and so on. The first four PCs capture already half of the total variance. The

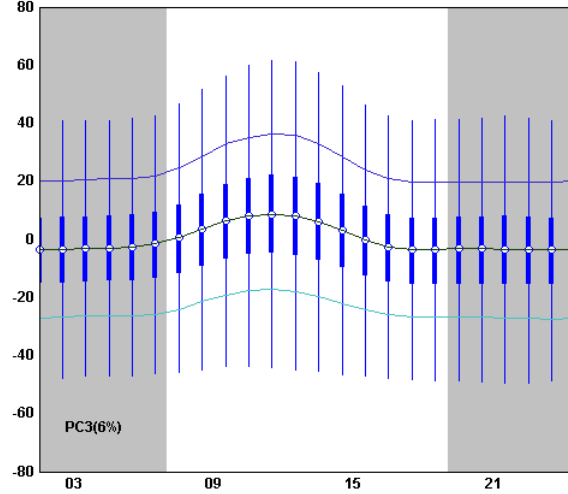


**Figure 10.** The diurnal cycle of PC3 for the cold season as a boxplot. The violet and green lines show the 90th and 10th percentile respectively.

areas in the maps with similar coefficient values exhibit the pattern captured in that particular PC. Basically, the red areas in the maps are out of phase with the blue areas and the percentage value can be thought of as a measure of importance of that PC. This first investigation set reveals high offshore variations whereas onshore variations are not sufficiently represented in the figure.

In order to increase the relative importance of the variations over land, we decided to use the z-score defined as:

$$z = \frac{x - \mu}{\sigma} \quad (10)$$

where  $x$  stands for the data considered, in our case, WPD,  $\mu$  for its mean and  $\sigma$  for the standard-deviation. Thus, the absolute value of  $z$  represents the distance between the raw score and the mean in units of the standard deviation. All the following studies will consider z-scores instead of the raw values.

Until now we looked at the whole data set of wind power resource over the 31 years. Since AO and NAO are generally much stronger during the cold season (Atkinson et al. 2006), we limited our data set in a second study respectively. Besides this helps us reducing calculation times and necessary memory space. We also conducted the analysis that follows reducing the data sets to the cold season over wider Europe. As the results are quite similar to the ones over core Europe we will focus on the latter ones. Looking at the PCs in time series, we identify strong diurnal cycles as shown for PC 3 for instance (see **Figure 10**).

In order to eliminate these diurnal cycles (since the available teleconnection indices are only available as at least daily means) we converted the hourly WPD data into daily averages for all following PCA studies.

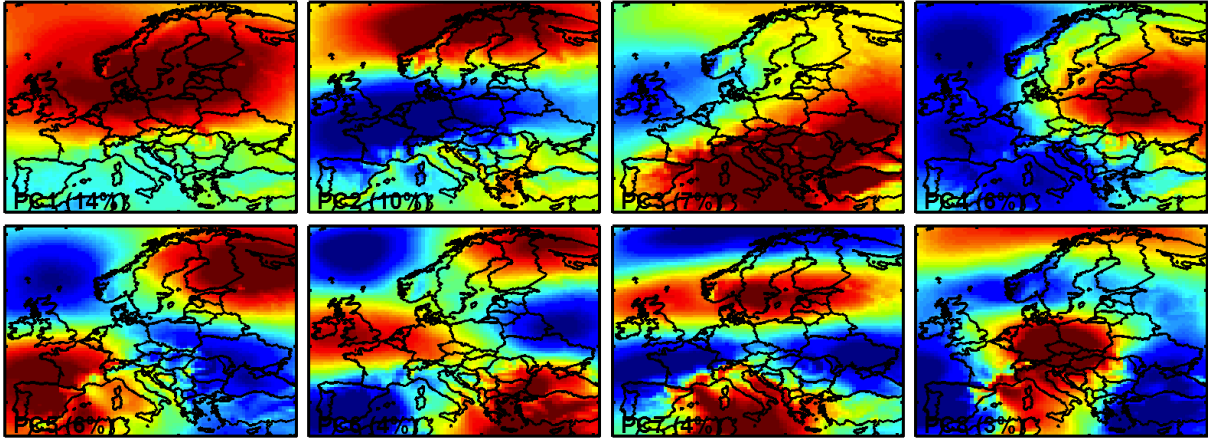


**Figure 11.** The first 8 PCs from the PCA of daily WPD over core Europe for the cold season. The values in parentheses are the percentage of variance explained by that PC. As before, the red areas in the maps are out of phase with the blue areas.

**Figure 11** represents the coefficients or eigenvectors of the eight first PCs for the cold season with daily averaged WPD data. In total there are 6080 PCs. The eight first components cover 54% of the total variance.

The most challenging part in PCA is the interpretation of each of the independent component. The analysis presented below provides quantitative insights in this regard.

#### *Correlation between principal components and teleconnection indices*

Our objective will be to find out if one of these PCs can explain variations due to teleconnections such as the NAO or AO. Therefore we started comparing the time series of the variation of the 50 first PCs with the time series of NAO and AO indices, both over the cold season during the same period of 31 years. We used a running mean of one year. Surprisingly the first and thus the most important PC is the only one to show great correlations for both NAO and AO. The AO index is represented by a green curve, the NAO by a red one. The respective time series for PC1, AO and NAO are shown below in **Figure 12**, the correlation seems slightly better for AO than for NAO. All the curves are normalized.

We assume that PC1 represents the impact of these two teleconnections. As shown before NAO and AO are highly correlated to each other and thus it is not surprising that both can be explained by the same PC. In order to verify this hypothesis we also calculated the cross-correlation sequences between the time series of each of the 50 first PCs of our PCA Analysis and the teleconnection indices. The cross-correlation coefficient sequences of the first four PC's are plotted in **Figure 13** for both AO and NAO.

We identify in both cases a high correlation coefficient for PC1 and PC3 in the middle. That means in the case without lead or lag of one signal on the other. There also seems to be a correlation between PC2 and AO. The correlation between PC2 and AO is not very high (0.15 at the

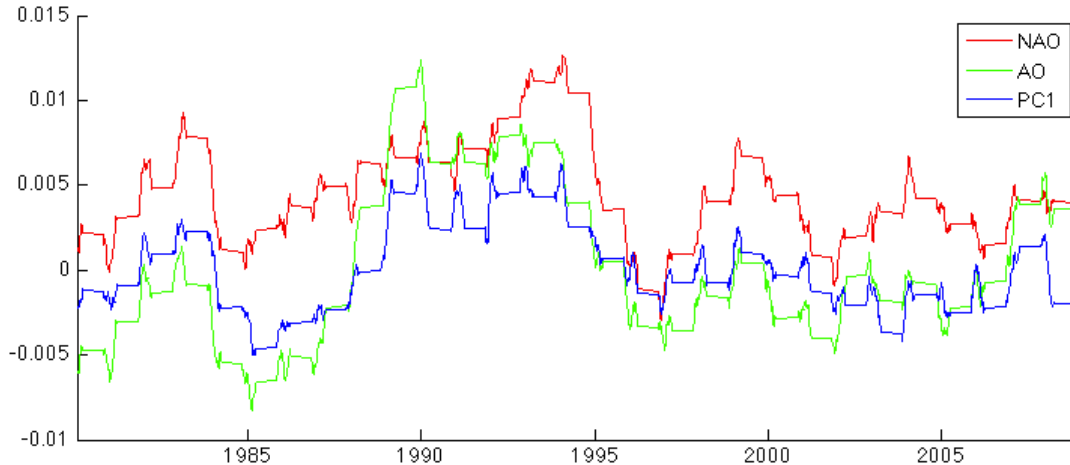


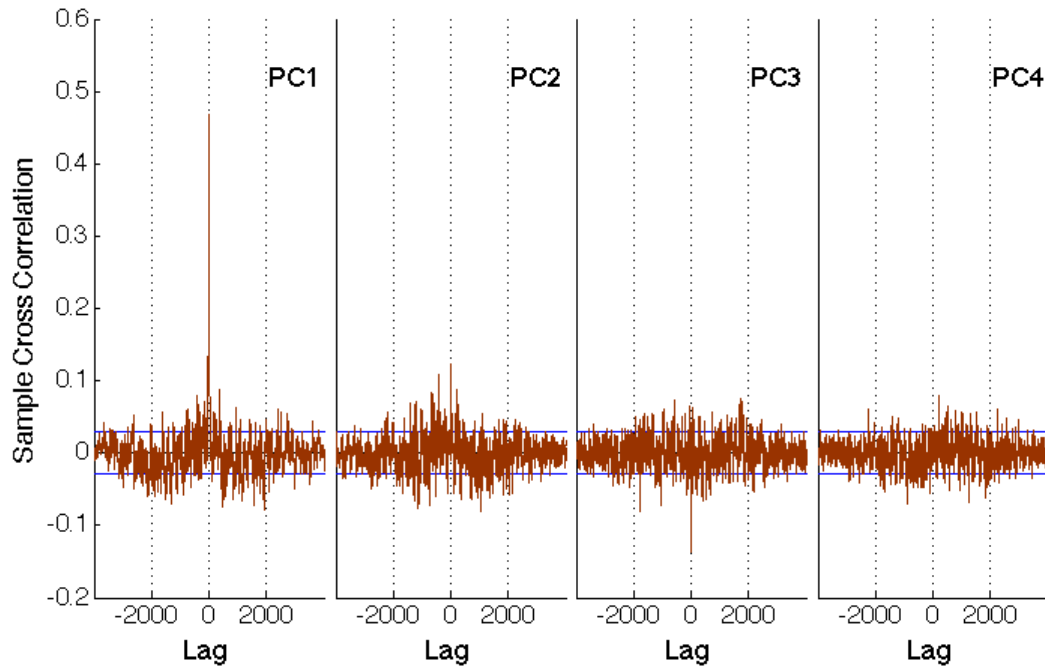
**Figure 12.** Normalized time series of PC1 (blue), NAO index (red) and AO index (green) for a running mean of one year over the 31 years of data for the cold season.

maximum), neither the correlation between PC3 and NAO/AO (less than -0.2 at the maximum). PC1 on the contrary has quite a high correlation with AO and NAO.

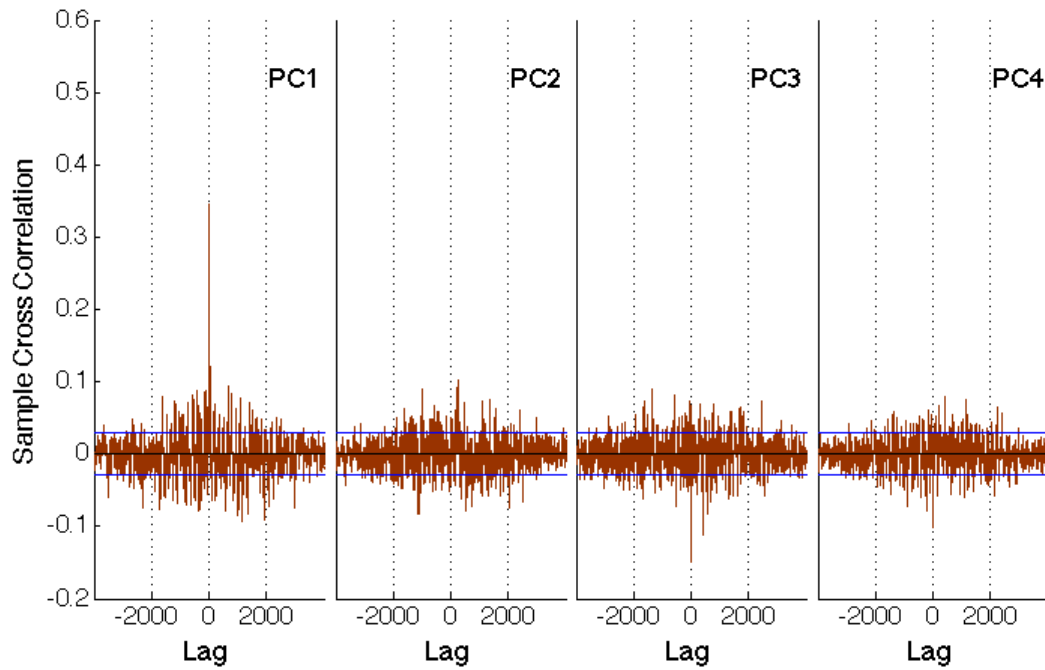
The highest correlation of 0.46 can be found between PC1 and AO, NAO's correlation with PC1 is 0.32. Besides, there is no significant lag or lead between the two curves. The maximum correlation is exactly in the middle of the sequence for both teleconnections. Further, we identify a maximum lead of NAO on the variation of PC1 of one day. We also calculated the coefficient of determination for a linear regression in the case of no lead or lag. Using a running mean over one year we obtain a  $R^2$  value of 0.736 in the case of AO and of 0.574 in the case of NAO. The  $R^2$  values are much lower but still significant at the 1% significance level if we use the raw (not smoothed) data: 0.219 in the case of AO and of 0.118 in the case of NAO. By definition these results are consistent with the  $r$ 's calculated above. For all the other PC's we get  $R^2$  values that are much smaller than 0.02 and thus not significant and negligible.

If we use the whole data set smoothed over one year instead of the limitation to the cold season we get a  $R^2$  of 0.226 for AO and of 0.159 for NAO. Thus, the limitation to the cold season is justified. A further reduction to the winter season results in slightly higher values for NAO and slightly lower ones for AO. This is fully consistent with Atkinson et al. (2006). Our results contradict Ambaum (2001) stating that only the NAO pattern can be identified in a physically consistent way in PCA applied to various fields in the Euro-Atlantic region, but no such identification is found for the AO. With WPD we found a field that can be well identified in PCA.

Unfortunately we were not able to diagnose as clearly as in the case of AO/NAO the other teleconnection indices studied such as ENSO, AMO and PNA in one of the PC's. Nevertheless, that underlines the importance of AO and NAO regarding WPD variation over Europe and explains why the focus of the present studies is on the latter ones.



(a) PC 1-4 and AO.



(b) PC 1-4 and NAO.

**Figure 13.** Cross-correlation sequences between the first four PCs and the respective teleconnection index. The blue lines indicate a confidence interval of 95%.

### 4.3 Influence of NAO/AO Indices on Wind Power Density

In this part we will try to prove the results of the previous chapter revealing a significant impact of AO and NAO on WPD that had been explained by the first PC accounting for 14% of the total variance of WPD. Therefore we will first look at the correlation between WPD time series and the respective teleconnection index and then give a more comprehensive measure of the impact of these teleconnections.

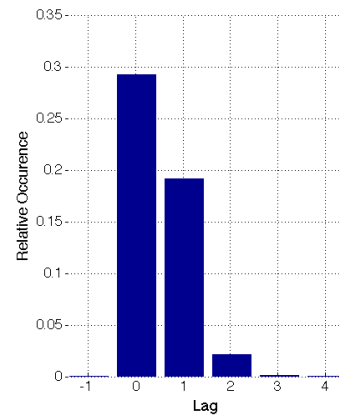
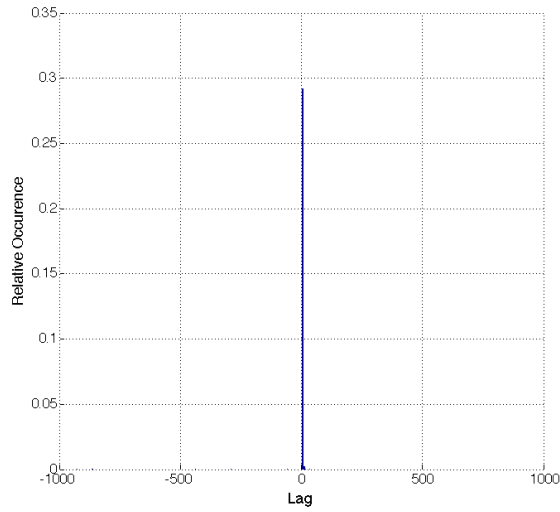
#### *Correlation between teleconnection index and wind power density*

**Lead of NAO and AO on WPD** In order to validate that there is no lag and a maximum lead of one day of the teleconnection on WPD we are studying the cross-correlation sequences between both time series. We will present our results for the cold season for every grid point.

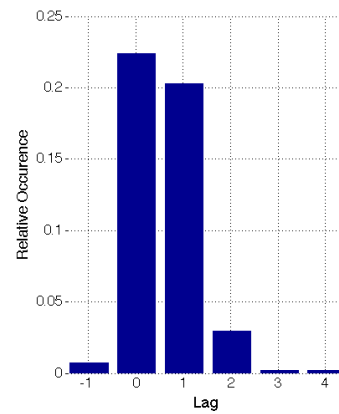
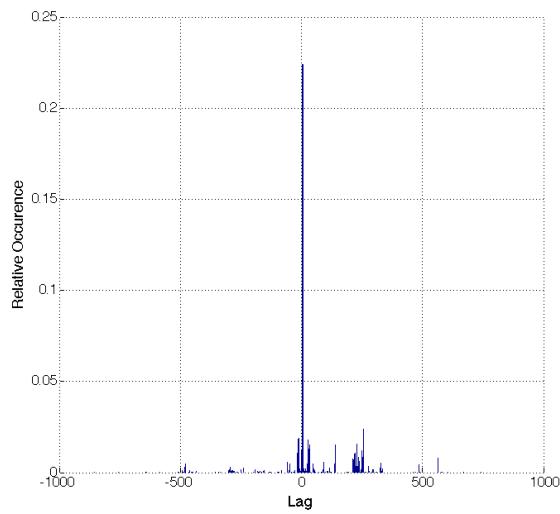
**Figure 14** shows the histograms of the lags of the cross-correlation coefficient sequence where the highest cross-correlation values can be found for every grid point. In both cases we observe a high peak in the middle around 0 lag. Looking at the histograms in detail we observe that in the case of AO, 29.2% of the grid points obtain their maximum correlation coefficient for a situation without lead or lag of the teleconnection on wind power resource (30.5% for the whole data set). Furthermore, 19.1% of the grid points have the maximum correlation at a lead of one day of the teleconnection on WPD (18.4% for the whole data set). In the case of NAO, 22.4% of the grid points have maximized correlation for the situation without lead (15.9% for the whole data set). A lead of one day can be observed for 20.2% of the grid points (15.9 % for the whole data set). Two days leads occur in less than 3% of the grid points in both cases. Thus, our results of the cross-correlation analysis of PCA component 1 are proved: 0-1 day lead in the case of AO and NAO.

It is also interesting to plot the number of lag-days between teleconnection and WPD for which the correlation coefficient is maximized at each grid point as it has been done in **Figure 15**. The big white area in northern Europe that can be found in both cases - AO and NAO - underlines the results stated above and reveals a large zone with similar pattern that had already been identified in the PCA (red area in **Figure 11**). The maximum lead of one day in both cases can be interpreted as a high persistence between AO/NAO and WPD and corresponds to what we could have expected. As a consequence it is important to monitor AO/NAO on a daily basis. Nevertheless, it makes it more difficult to react on AO/NAO changes and to adapt wind power generation for instance. Thus, the prediction of these indices as far in advance as possible becomes an important issue.

In addition, the result of only one or even zero lag was confirmed by mapping and comparing the geographical variation of each situation with lags between 0 and 10 days. The zone of high correlation in northern Europe is getting smaller and less intense with increasing number of lag



(a) AO



(b) NAO

**Figure 14.** Histogram of the delay between WPD and AO (top) and NAO (bottom) for which a maximum correlation can be obtained. Positive x-values correspond to a lead of NAO on WPD, negative ones to a lag. Both are measured in days. The figures on the right represent a zoom into the lags of interest in the left figures.

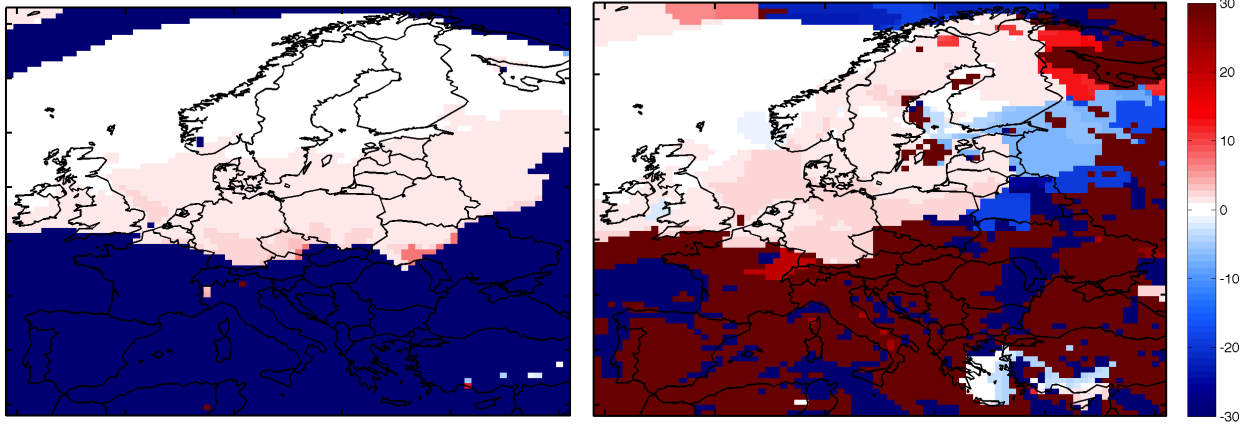


**Figure 15.** Geographical variation of lead days of maximum correlation between AO (left) and NAO (right) and WPD. The scale is reduced to  $\pm 30$  days of lead/lag. As a result, all higher and lower values appear as the extreme values.

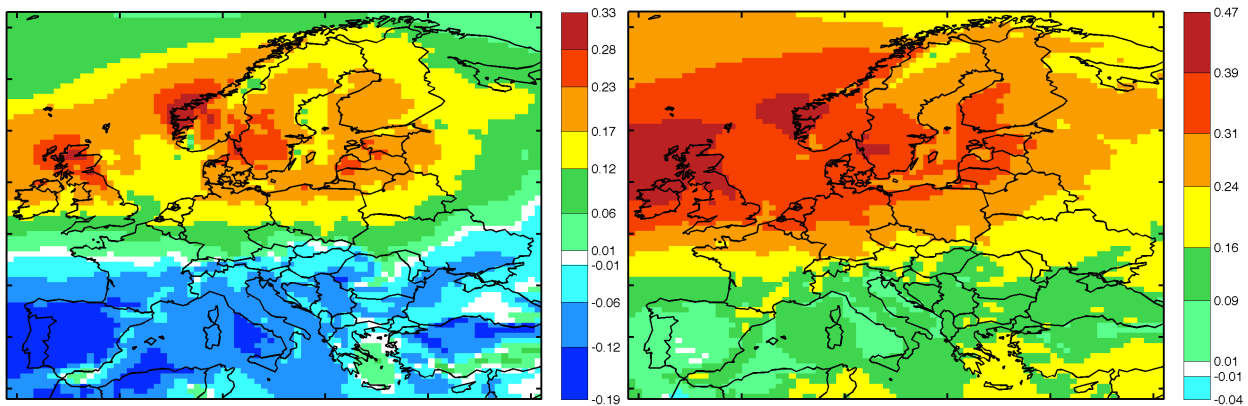


**Figure 16.** Geographical variation of the cross-correlation coefficient at a significance level of 1% in the case of AO (left) and NAO (right) without lag/lead. As before we considered the cold season.

days.

**Correlation between NAO/AO and WPD** Not surprisingly the cross-correlation plots for zero and one day lag are almost the same for both AO and NAO, thus we are only presenting the ones in the case of no lag in **Figure 16**.

It is important to note that AO and NAO are both highly correlated with WPD for northern Europe, especially northern UK, coastal Norway and southern Sweden, whereas the correlation is much weaker for southern Europe. In the case of AO we observe even a negative correlation for southern Europe. It is highest over Spain. All the plotted correlation coefficients are significant at a confidence level of 99%. These results correspond exactly to what we have seen in PCA, where the Eigenvectors of PC 1 were best aligned for a large zone in northern Europe. Nevertheless, PCA revealed higher correlation between PC1 and teleconnection for AO than NAO, whereas the



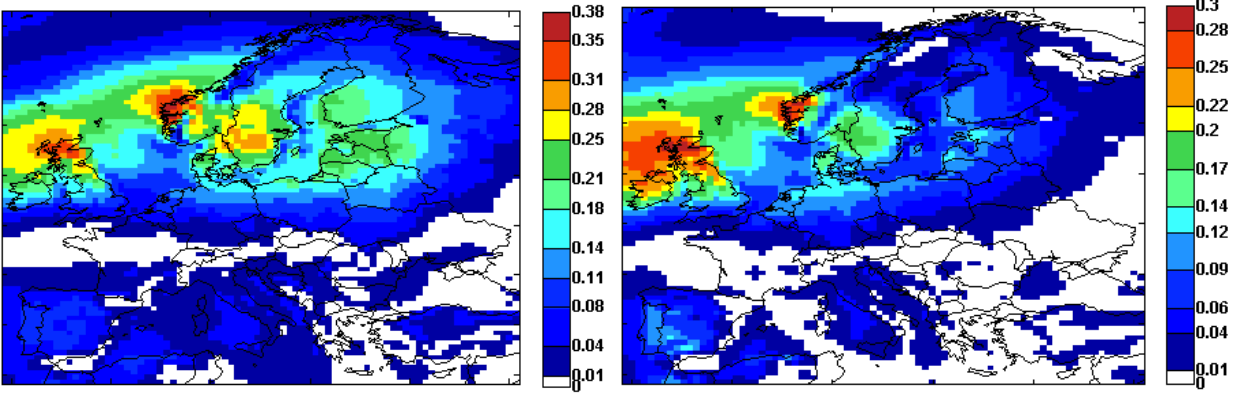


**Figure 17.** Geographical variation of  $R^2$  using a linear regression between teleconnection index (AO on the left, NAO on the right) and WPD for the cold season for a running mean over 1 week. The coloured values passed a slope test at a significant level of 1%. Non-significant values are plotted in white.

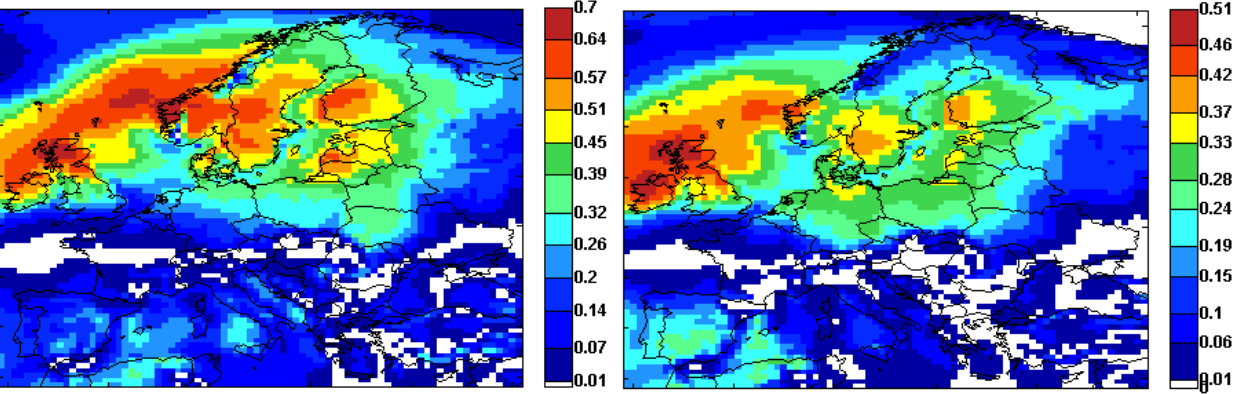


**Figure 18.** Geographical variation of  $R^2$  using a linear regression between teleconnection index (AO on the left, NAO on the right) and WPD for the cold season for a running mean over 20 weeks. The coloured values passed a slope test at a significant level of 1%. Non-significant values are plotted in white.

correlation between WPD and teleconnection appears to be higher for NAO<sup>1</sup>.

Smoothing the data used can significantly increase the correlations. For example, for the cold season we obtain correlations up to 0.8 and 0.75 for AO and NAO respectively if we apply a running median of a year to both teleconnection index and WPD.

The  $R^2$  value was also considered (**Figure 17** and **Figure 18**) since it provides a physical interpretation of the correlation coefficient as part of the variance of WPD that can be explained by the respective teleconnection.

***Impact of different states of the teleconnection***

Since we can be confident now that a significant correlation exists between AO/NAO and WPD we want to quantify the effect of a changing phase in the teleconnection index in terms of

<sup>1</sup> If we consider only the winter season the correlations get about 5% higher for both AO and NAO. Taking into account the whole data set on the contrary has the opposite effect and correlations decrease by about 40%. Nevertheless, the geographical variation stays in all data sets qualitatively the same.

increase or decrease of WPD. As a comprehensive way to do that we chose to divide each teleconnection index into three states: positive, medium and negative. The limits between these states are carefully chosen in order to create bins of equal number of data elements. For each grid point the WPD at a time  $t$  over the cold season is categorized into one of these three levels depending on the state of the teleconnection at the same time. As a result we obtain a sample of WPD that occur for high or positive NAO/AO as well as one for low or negative NAO/AO. Since we know that there is a maximum lead of one day of teleconnection index on WPD we applied a two-day moving average on the teleconnection time series. In the following we are going to analyze these samples and in particular their relative variations due to a change of the teleconnection phase. As already stated above, the histogram of WPD at a certain grid point is highly skewed and a long-tailed distribution. Thus, the mean may not faithfully represent the distribution's central tendency of the WPD accurately. As a consequence, we should rather consider the median.

**Geographical variation in WPD** Let us first look at the impact of the AO. WPD varies up to 2 times between phases of positive and negative AO. The variations are much stronger for the median than for the mean values as shown in **Figure 19** and **Figure 20**. It is important to underline the high confidence level of 99% that has been obtained using a two-tailed t-test for statistical significance (see appendix). In the case of positive AO, median WPD increases of about 30–200% for north western Europe, whereas southern Europe is characterized by a decrease of about 30–40%. The highest increases can be observed for northern Great Britain and the north west coast of Norway. This different pattern of variation in WPD between the North and the South reveals a high potential for interconnection between wind farms in order to reduce intermittency and to balance the variability of the resource. For instance, in the case of a change of the AO phase from negative to positive the higher amount of generated power by a wind farm located in the North could be used to compensate the lack in wind energy generated by a southern wind farm. If AO turns negative again the opposite will happen and the North can be balanced by the South. Since the probability of apparition of each state of AO equals one third we can further say that this high interconnection potential can be exploited at least two third of the time. Nevertheless, an increase in intensity of WPD due to high AO/NAO is always associated with an increase in standard deviation. Consequently, the WPD distributions get much wider and the risk occurs that only a small percentage of the WPD can be converted to electricity since power curves are only defined for a limited interval of WSs (see 3.3).

In the case of the NAO our results are quite similar to the ones stated above for AO. Nevertheless, regions with decrease of WPD in the South seem to be less widespread and weaker. Besides the area with increase of WPD is more located in the North West. Quantitatively, the increases are slightly lower. Nevertheless, a similar potential for interconnection between wind farms can

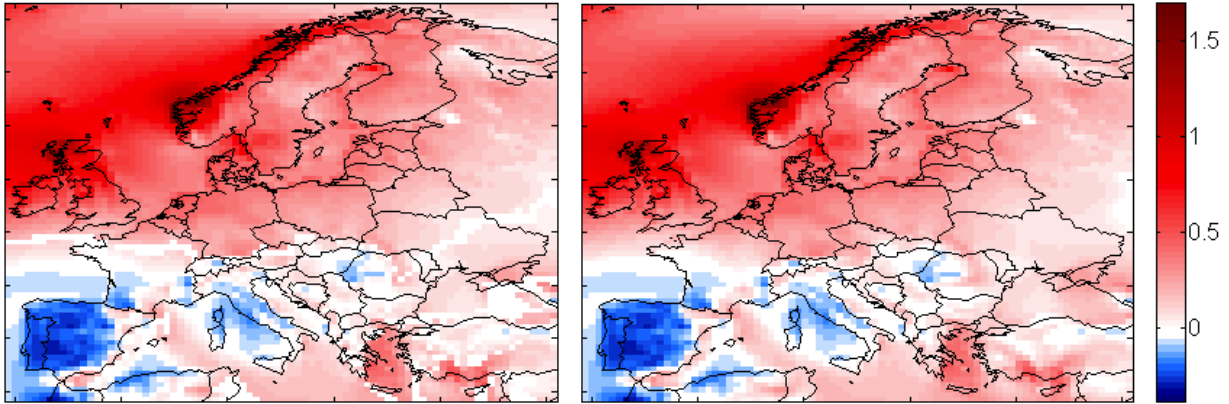


**Figure 19.** Relative variation in mean WPD at a significance level of 1% if AO (left) or NAO (right) changes from the negative state to the positive one.

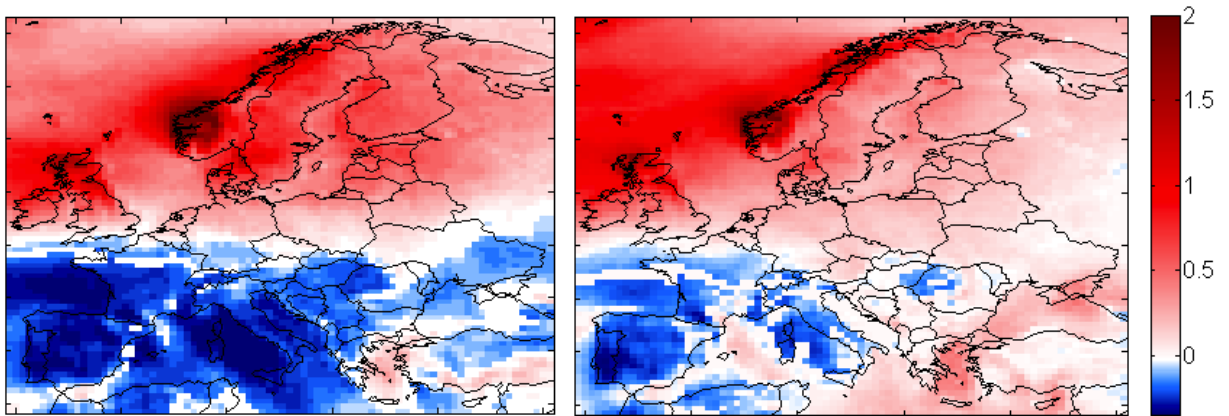


**Figure 20.** Relative variation in median WPD at a significance level of 1% if AO (left) or NAO (right) changes from the negative state to the positive one.

be noted. Again, **Figure 19** and **Figure 20** are completely consistent with the areas of similar pattern identified in the first PC in PCA.

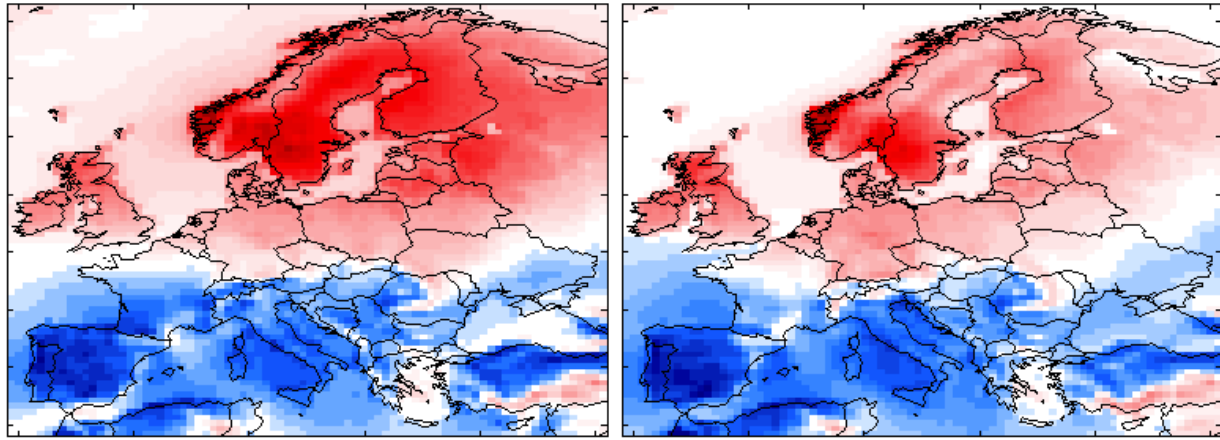
It is difficult to compare our results with the previous studies by Brayshaw (2011) and Jerez (2013) given that we are looking at WPDs whereas they use WS distributions to assess the potential energy output by a hypothetical wind turbine. In our case high WS result in high WPD. Nevertheless, as already mentioned the generated power by a turbine depends on the respective power curve. It can be that WSs are too high and consequently fall outside of the operable range of WSs for the chosen turbine that would remain inoperable most of the time.

**Geographical variation in generated energy output** Given these limitations we would like to do the same study as before, comparing the impact of different phases of the teleconnections. But this time we will look at the real energy output by wind turbines instead of WPD, that should rather be considered as a potential upper bound of energy that could be extracted. We will do that for every grid point over core Europe. Furthermore, we will not only consider one hypothetical

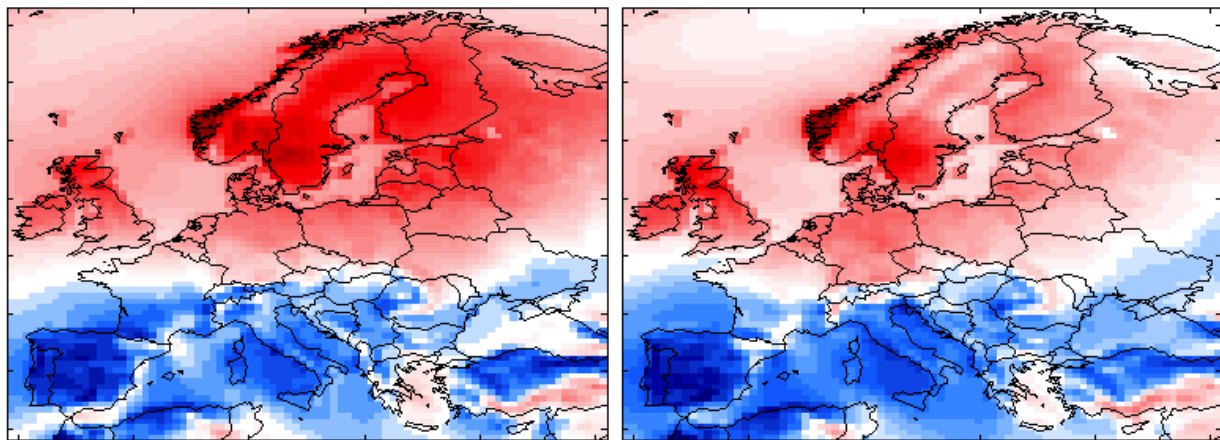
wind turbine as done by Brayshaw et al. (2011) but three different ones (see 3.3). Model 2 corresponds to the wind turbine used by Brayshaw.

**Figures 21a-c** show the relative differences in generated energy between positive and negative phases of both AO and NAO for each model wind turbine. In all of them we identify an important north-south difference confirming the high potential of interconnection between northern and southern Europe that has already been stated before when looking at WPD. It seems to be stronger for AO than for NAO. Effectively, in the case of a positive AO phase, up to 200% more electricity can be generated in the North compared to a negative teleconnection phase whereas the generation in southern Europe decreases by about 40–50%. Not surprisingly, the three plots for AO look really similar independently from the wind turbine used. The same can be observed for the plots for NAO. This result is really meaningful since it tells us that independently from the wind turbine used there will always be a high potential for interconnection between wind farms between the North and the South. The plots for Model 2 and 3 seem to be almost the same. That can be explained by the similar power curve for these two turbines. Comparing Model 2 and 3 with Model 1 we observe certain differences, especially in the offshore regions.

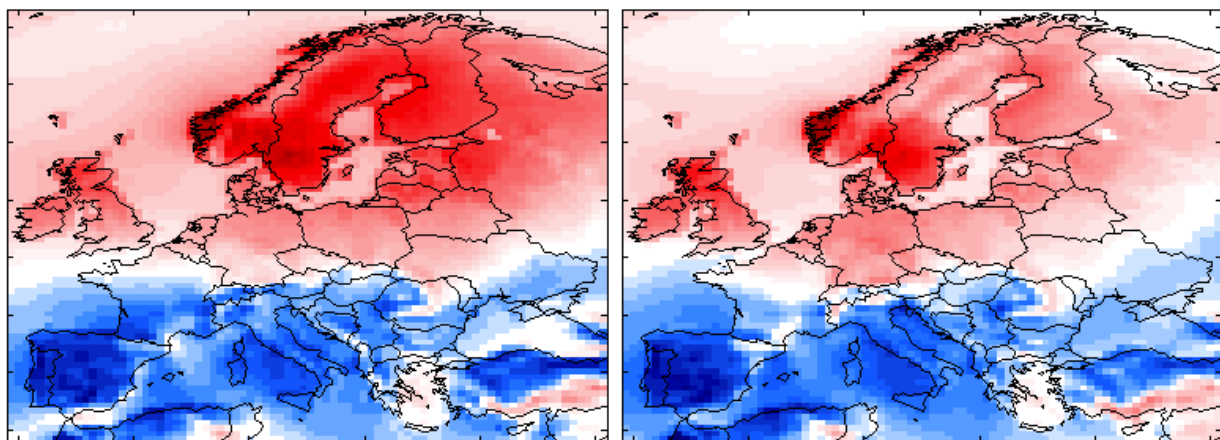
It is interesting to compare our results with the ones of Brayshaw (2011), therefore we plotted in **Figure 22** on the left a zoom on the UK for wind turbine Model 2 that corresponds exactly to the one used by Brayshaw. We obtain qualitatively the same results as Brayshaw who found that energy output at the two locations that have been studied increases by 18.6% in STO, the coastal airport on an island in the north west of the Scottish mainland, and by 11.3% in GDF, an exposed land area in the center of the UK in the case of positive NAO compared to the negative phase. Furthermore, they stated that the same study for London Heathrow revealed a much weaker relationship between WS and NAO. Nonetheless, quantitatively our results show higher increases of the wind power output: 60% for STO and 40% for GDF. This difference can be explained by the different methodology applied as well as by the different data sets used. For instance Brayshaw obtained its data at 80 m heights by multiplying the 10 m WS by a constant scaling factor that had been chosen with a certain arbitrariness. Therefore, the resulting power output should be interpreted with caution. Nevertheless, our results over Portugal and Spain are completely consistent with Jerez et al. (2013) as shown in **Figure 22** on the right. They state that a negative NAO phase enhances wind power by about 30%. This is extremely encouraging since Jerez used data over a period of 48 years with a more than five times higher spatial resolution.



(a) Model 1



(b) Model 2



(c) Model 3

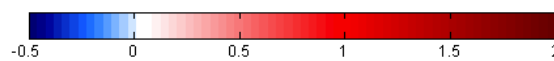


**Figure 21.** Relative variation of the energy output between positive and negative AO (left) and NAO (right) phase for each of the three wind turbine models considered. Red and blue areas represent respectively increase and decrease of the generated energy due to the change from a negative to a positive teleconnection phase.

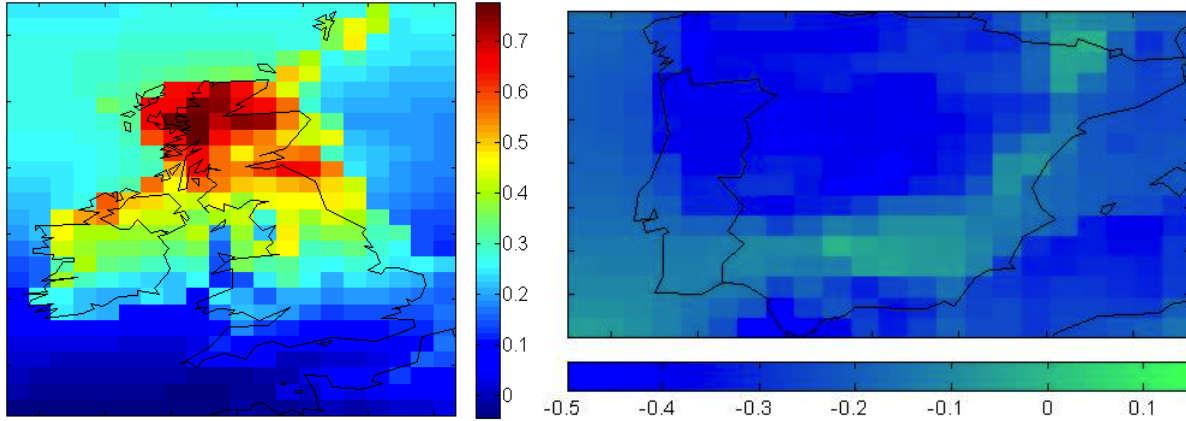


**Figure 22.** Relative variation in energy output over the UK using Model 2 (left) and over Spain and Portugal using Model 3 (right) if NAO changes from a negative phase to a positive one in order to compare them with the results of Brayshaw (2011) and Jerez et al. (2013).

**Table 2.** Some approximative annual total energy outputs by a model turbine depending on its location and the phase of AO.

Wind turbine (max. output [GWh])	<b>Model 1 (17.5)</b>		<b>Model 2 (26.3)</b>		<b>Model 3 (28.9)</b>	
Location	North	South	North	South	North	South
Positive AO	9-12	1-5	13-16	1-6	15-19	2-9
Negative AO	7-9	3-8	8-10	3-10	10-13	5-12

**Table 2** provides some absolute values for the annual energy that can be generated by one wind turbine depending on its location and the phase of AO for instance. The values are quite similar for NAO. We use northern UK and Spain as example locations in the North and the South respectively. The values in brackets after the turbine model indicate the maximum possible annual power output by this turbine and can be used to calculate the CF. It is important to note that the indicated values are only approximations in order to give an idea of the absolute quantities since we were only looking at relative differences so far.

We see that high CFs can be obtained in the North in the case of a positive teleconnection phase, whereas these are really small for the southern regions. When the phase turns negative, CF's in the South increase significantly whereas the CF's of northern wind farms decrease.

Similarly, **Figure 23** shows in absolute values over whole Europe how much more or less energy can be generated by wind turbine Model 3 if AO/NAO changes from a negative state to a positive one.

In order to well represent the generated energy output by installing a wind farm at a certain grid point it is important to estimate the number of wind turbines that could be installed in the area around a grid point. This area can be modeled by a rectangle of 50 km x 66,7 km. We assume that only 10% of the grid cell area can be used for wind turbines due to other land uses or constraints. Meneveau and Meyers (2010) found that the spacing between turbines should

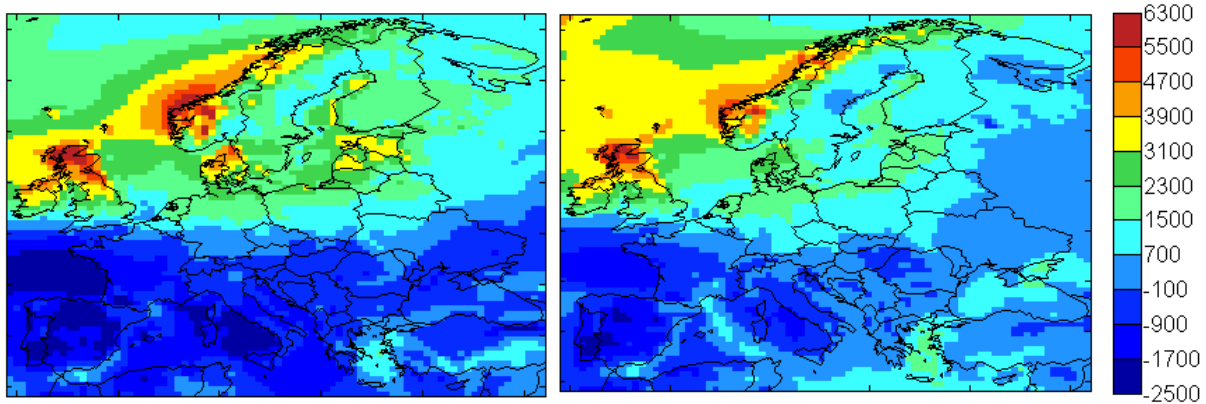


**Figure 23.** Difference in the energy output generated by Model 3 in MWh during a positive and a negative phase of AO (left) and NAO (right).

be about 15 rotor diameters to maximize cost effectiveness. This spacing is much higher than that applied in conventional wind farms (7 rotor diameters). For instance, Model 3 of the used wind turbine has a rotor diameter of 112 m, thus there should be a distance of 1,68 km to its next neighbour turbine. In our estimation we try to cover the rectangle around the grid point with as many circles of radius 840 m as possible using a honeycomb model. As a result we obtain an optimal number of 14 turbines per grid point for Model 3. As a consequence, the energy output in **Table 2** should be multiplied with the respective optimal number of turbines in order to estimate the electricity that can be generated in total over one year at one grid point. The optimal number of turbines at one grid point for Model 1 (rotor diameter: 100 m) and Model 2 (rotor diameter: 90 m) are about 18 and 16 respectively.

Finally, we should keep in mind that besides the relative increase/decrease in generated energy output due to a change of the respective teleconnection phase, a minimum WPD is required at every site for which interconnection should be applied to balance variability during at least one of the extreme teleconnection phases. Gustavson (1979) found that at least a WPD of  $220 \frac{W}{m^2}$  is needed for minimum usable wind power generation. In the U.S. Wind Resource Atlas (Elliott et al. 1987)  $200 \frac{W}{m^2}$  was used as the minimum WPD for usable power production. Given the important technological advances in the last decades we will consider a threshold of  $180 \frac{W}{m^2}$ . The colored areas in **Figure 24** (right) are the potential candidates for interconnection between wind farms with a minimum mean WPD of  $180 \frac{W}{m^2}$  in at least one of the extreme phases in the case of AO:

- green: the threshold is only obtained for a negative phase of the teleconnection
- orange: the threshold is only obtained for a positive phase of the teleconnection
- blue: the threshold is obtained for both extreme phases of the teleconnection

We observe that this necessary requirement is only fulfilled for specific regions. To reduce inter-

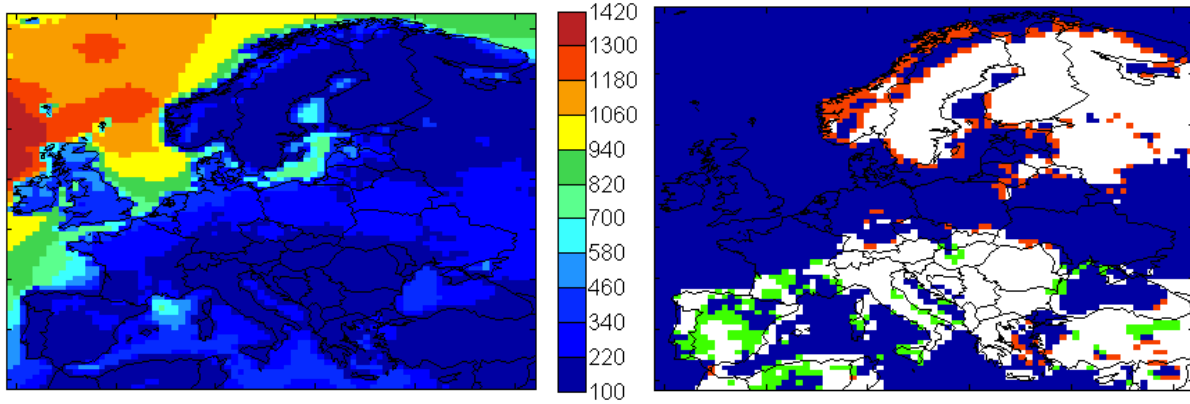


**Figure 24.** Left: Mean WPD in  $\frac{W}{m^2}$  in Europe over the whole year; Right: In colors: Potential candidates for interconnection with a minimum mean WPD of  $180 \frac{W}{m^2}$  in at least one of the extreme phases for AO during the cold season.

mittency, it would be optimal to interconnect the red points with the green ones. Interconnecting the blue points will rather balance variability than intermittency and should thus also be an objective. Nevertheless, it has to be noted that this criteria provides only a general idea of potentials but that more detailed local studies should be conducted in order to choose the right regions for interconnection. **Figure 24** (left) shows the geographical variation of mean WPD over Europe.

In addition, a detailed study about the feasibility of interconnection should be done for these regions. Therefore the costs of the losses by transmissions of electricity as well as the necessary investments to install an interconnected grid should be evaluated against the benefits due to reduced intermittency and better balanced variability. In its Energy Infrastructure Package the European Union considers the north-south interconnections in Central and South Eastern Europe as a priority (EC). Our results presented above confirm that this interconnection project will help reduce intermittency due to AO/NAO. Nevertheless, the majority of the south eastern countries does not fulfill the minimum WPD requirement stated above. Our study shows that there are much better potential countries for interconnection if we aim to balance the impact of AO/NAO, especially the most northern ones such as England and Norway and the Mediterranean ones. An interconnected electricity grid covering all of Europe should be the objective to balance best the teleconnectivity of AO/NAO and consequently reduce variability by as much as 30% during the cold season for the North, for instance.

#### 4.4 Explanation of the Impact of AO/NAO

While almost no literature is available explaining the impact of AO on European climate, several studies have established links between different NAO modes and changes in the associated activity of North-Atlantic storm tracks. According to Ulbrich et al. (1999), the NAO is closely associated with the intensity of the Atlantic storm track's extension into Europe. A change of



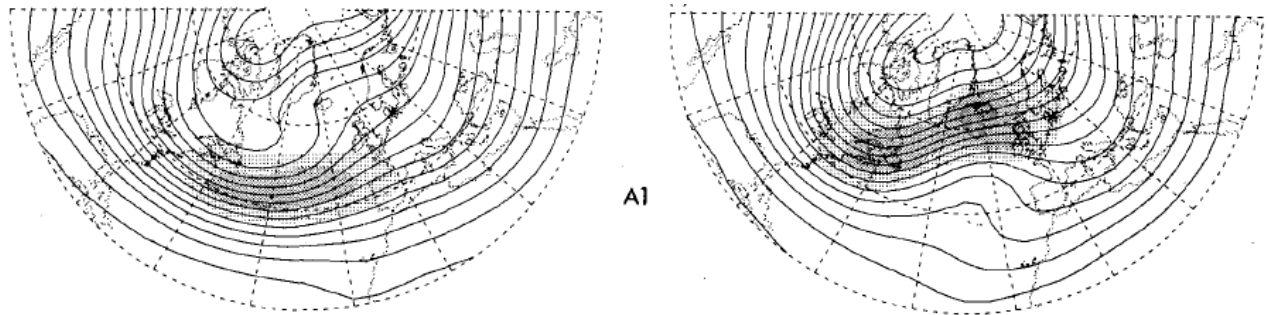


**Figure 25.** High (left) and low (right) composites of the first principal Atlantic storm denoted A1. This mode is negatively correlated ( $r = -0,61$ ) with the EA teleconnection (source: Lau 1988)

the NAO pattern results in a steadily growing storm track activity over north western Europe. In addition, they predicted a systematic northeastward shift of the NAO's northern variability center from the east coast of Greenland to the Norwegian Sea during the subsequent 10 years. By applying EOF analysis of the monthly root-mean-square statistics of bandpass filtered (2.5–6 day) twice-daily 500-mb geopotential heights, Lau (1988) identified storm track modes over the North Atlantic and was able to link them to the eastern Atlantic teleconnection patterns found in monthly time averages (**Figure 25**). He proved that the eastern Atlantic teleconnection pattern, also called “southward shifted NAO pattern“ (NOAA), is coincident with a north-south displacements of the storm track axis by as much as  $20^\circ$  of latitude over the eastern Atlantic. Further the characteristic circulations at sea level shown in a composite chart of the SLP field associated with the first principal mode resemble the patterns associated with the NAO.

Equally, Baldwin and Dunkerton (2001) suggest based on their observations that large circulation anomalies in the lower stratosphere are linked to substantial shifts in the AO and NAO. They showed that over the Atlantic sector the storm track is displaced significantly farther south in the case of weak vortex regimes, compared to strong vortex regimes. Interestingly high AO or NAO indices occur with a three to four times higher probability during strong vortex regimes than weak vortex regimes. The opposite is observed for low indices. Besides, the observed circulation changes during weak and strong vortex regimes can be anticipated by observing the stratosphere. These results imply a measure of predictability, up to two months in advance, for AO/NAO variations in northern winter, especially for extreme values.

Rogers (1997) also states that the NAO may be closely associated with the latitudinal aspects of storm track variability in the central Atlantic, but that the low-frequency teleconnections that are linked to the predominant mode of the storm track variability in the North Atlantic are in the far northeastern Atlantic, what is completely consistent with our results. Furthermore, Hurrell (1995) showed that in the case of high NAO during winter, the westerlies onto Europe are over  $8\frac{m}{s}$  stronger than for low NAO winters.

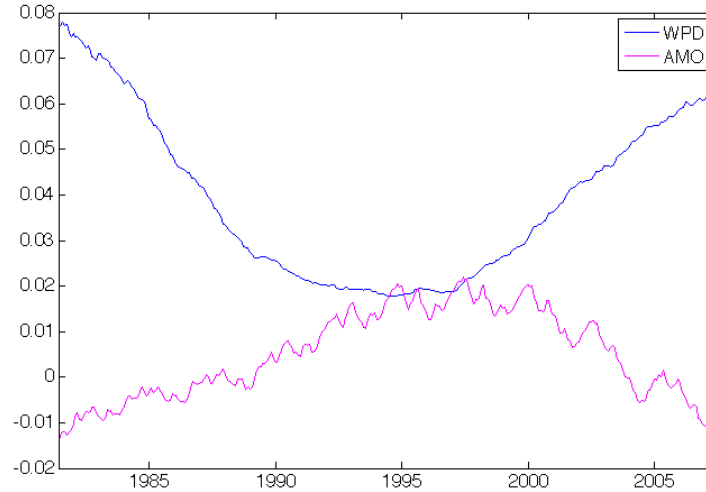


**Figure 26.** Normalized time series of monthly AMO and monthly mean WPD over Munich (GER).

To conclude, we can explain the influence of AO/NAO on WPD by three effects occurring in the case of a high phase of the teleconnection:

1. Much stronger westerlies
2. Intensification of the Atlantic storm tracks
3. Shift in the North Atlantic storm tracks resulting in enhanced winds toward the north western oceanic area and weakened winds throughout most of the European continent

#### **4.5 Influence of the Atlantic Multidecadal Oscillation on Wind Power Density**

Similarly to our studies on AO/NAO and WPD we are interested in assessing if there is also an impact of AMO on WPD. If yes we would like to quantify it. Since AMO is a multidecadal pattern we are using in the following a running mean of 5 years in order to get the long term trend and reduce noises. Besides we will this time consider wider Europe. Let us first look at the normalized time series of monthly AMO and monthly mean WPD for the whole data set at an example grid point: Munich (48.1°N, 11.6°E), shown in **Figure 26**. Both time series seem to be highly anti-correlated.

##### ***Atlantic Multidecadal Oscillation and Principal Component Analysis***

Comparing the time series of AMO with the first 8 PCs does not result in a clear identification of any PC as this has been the case for AO/NAO. Several PC's show high  $R^2$  for a linear regression: PC1: 0.48, PC2: 0.53, PC3: 0.45, PC5: 0.40, PC7: 0.43, PC8: 0.40. Unfortunately these values are not even significant at the 5% significance level if we use a slope test as described in the appendix. As a result we do not know if AMO can be explained by PCA.

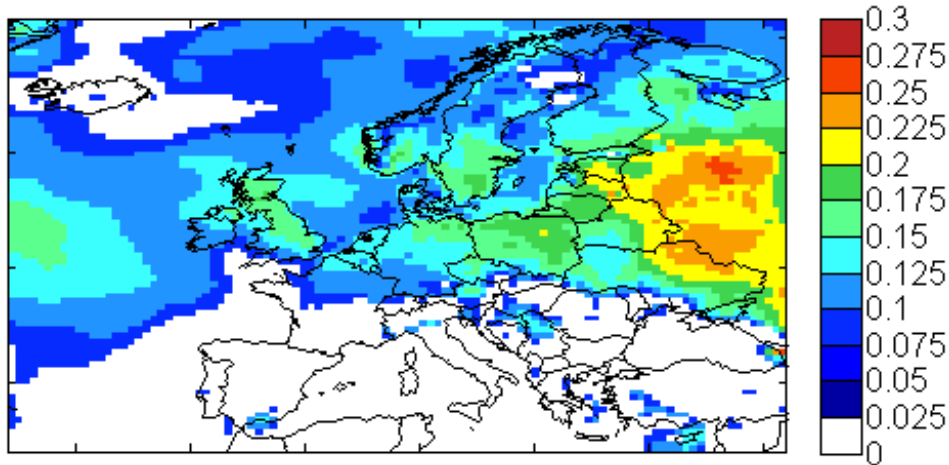


**Figure 27.** Coefficient of determination for linear regression between monthly AMO and WPD data using a slope test at 5% significance level. Non-significant values are plotted in white.

### *Correlation with wind power density*

Since correlation studies did not let us conclude about a lead or lag between WPD and AMO, we calculated the coefficient of determination at each grid point and only plot the significant values using a significance level of 5% (**Figure 27**). We prove that there is a certain correlation between WPD and AMO for northern Europe. Correlations appear to be higher over land than over sea. It is important to state that correlation is not causality. The fact that we observed a certain anti-correlation between WPD and AMO does not necessarily mean that one causes the other. It could be that both effects are caused by another factor.

### *Impact of different states of the large-scale climate variability pattern*

As we did before for AO/NAO we also categorized AMO into three phases: positive, medium and negative. Each phase occurs with a probability of 1/3. For each one we calculated a mean WPD and studied its variation in the case of a change between negative and positive AMO phase. A two-tailed t-test showed that our results in **Figure 28** are significant at a confidence level of 90%. We observe a decrease of mean WPD in the case of a positive AMO index compared to a negative one for almost all of Europe. Surprisingly, a high increase of mean WPD of up to two times arises for eastern Turkey and northern Syria.

As noted above it could be that the variation in AMO is a result of the variation in WPD. A higher WS over the Atlantic Ocean could favor higher convection and thus result in a cooling effect, whereas stagnant air or really low WS could cause a warming of the sea surface temperature.

To conclude, our results are consistent with Sutton and Hodson (2005) who showed that AMO variations have an impact on Europe's climate system, but that it is relatively small.

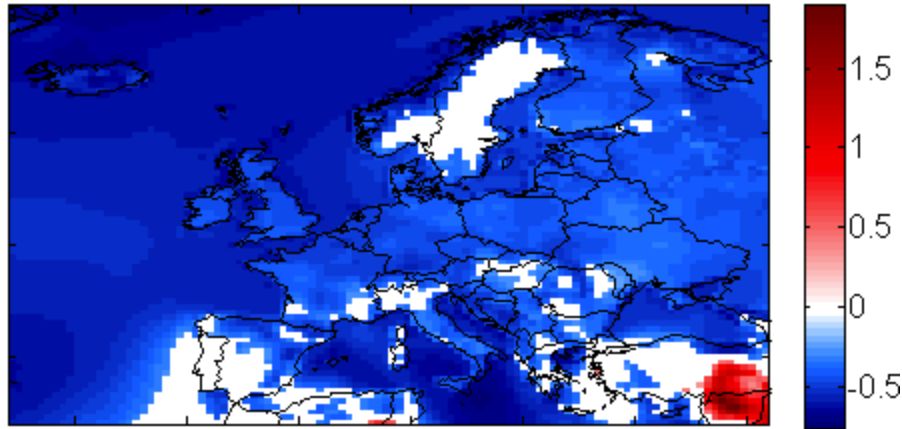


**Figure 28.** Relative variation of mean WPD if AMO turns from a negative to a positive phase. Non-significant values ( $\alpha = 10\%$ ) are plotted in white.

#### 4.6 Influence of the El Niño Southern Oscillation on Wind Power Density

In this part we present analogue to the previous chapter the results of our studies on ENSO. Since we only have monthly averaged ENSO indices, we used the monthly averaged data over wider Europe during the cold season. Unfortunately no significant correlation has been found neither between any PC and ENSO index nor between ENSO index and WPD data. Interestingly we observe a similar north-south pattern as identified for AO/NAO if we categorize the WPD data into events of strong positive and strong negative ENSO phase with a equal probability of occurrence of 1/3. **Figure 29** shows the relative variations of mean WPD if ENSO changes to a strong positive phase for two significance levels: 10% and 30%. As before a two-tailed t-test was applied. In addition to these low significances, the variations are very small ranging form -15% to +30%. Similarly to our conclusions in the part about AO/NAO, we can note a certain potential of interconnection between wind farms in northern Europe, e.g., Germany or northern France and wind farms in certain areas of the Mediterranean region such in Spain, southern France or Italy. These results are completely consistent with the previous studies that have stated a relatively small effect of ENSO in Europe.

### 5. CONCLUSIONS

In the present study the impact of several teleconnections and large-scale climate variability on wind energy resource over Europe have been evaluated and, if possible, quantified. Best results have been obtained for the AO and NAO teleconnections, especially in winter. Since much of Europe sees a maximum point-wise temporal correlation with AO/NAO leading WPD by at most one day it is important to monitor AO/NAO on a daily basis. Generally, the correlations between WPD and teleconnection index are slightly higher for NAO. From the PCA analysis we can infer that as much as 14% of the overall variation of WPD over Europe is explained by AO/NAO.

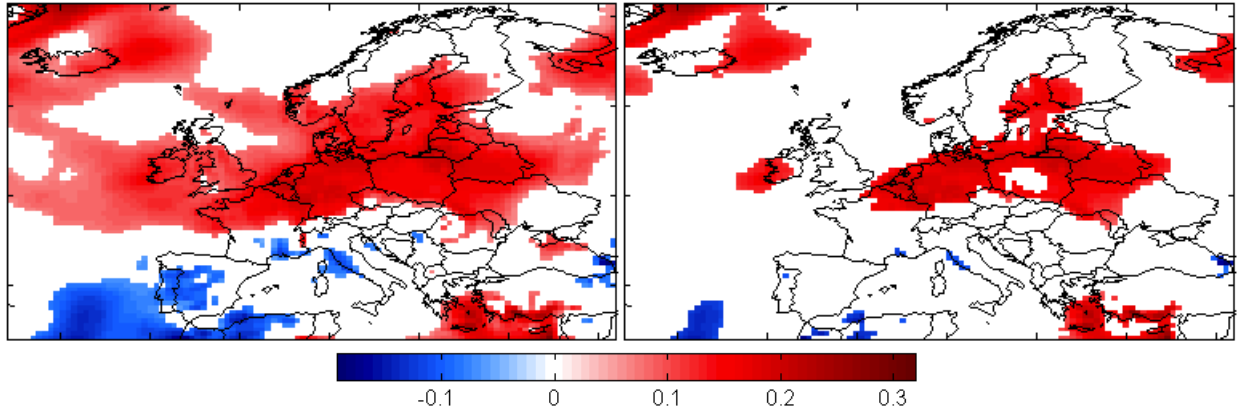


**Figure 29.** Relative variation at a confidence level of 70% (left) and 90% (right) of mean WPD if ENSO changes from a positive to a negative phase. Non-significant values are plotted in white.

This result has been confirmed by calculating the coefficient of determination for linear regression between WPD time series and the teleconnections over all of Europe. For northern Europe up to 30% of the variation of WPD can be explained by NAO, for example. In the case of high AO/NAO, WPD can get up to three times higher in northern Europe compared to a low teleconnection phase. The opposite effect can be observed for southern Europe; WPD decreases here by up to 50%. This different variation due to AO/NAO across Europe reveals a high potential for interconnection between wind farms in order to balance their variability and to reduce intermittency, one of the greatest challenges facing widespread deployment in wind power generation. Our study of the generated energy output using three types of model wind turbines provides a more realistic measure to prove this high interconnection potential, and shows that it is independent from the wind turbine used. Furthermore, predicting AO/NAO, can significantly help wind farm operators adapt to future wind power variations and stabilize wind power output throughout Europe, for example, by providing the right back up technology for lost wind power e.g. in the south of Europe when a positive phase of AO/NAO occurs. As a consequence, taking into account our results, wind power can become a more reliable and less intermittent resource that will help its expansion across Europe.

Compared to studies on the influence of teleconnection on wind resource over Europe that have been conducted before, it is important to note that our study is the first to look at WPD on a large scale. Our study also provides a more comprehensive analysis since we include air density and are thus able to estimate the upper bound of wind power that can be generated independently from the wind turbine used. In addition, we estimated the effective energy output for every grid point over all of Europe for several wind turbines of different scales. In order to validate our results, the scripts developed to study AO/NAO have also been applied to other teleconnections such as the Pacific North Atlantic Oscillation (PNA). Not surprisingly we observed absolutely no correlation in this case. Furthermore, our results for ENSO and AMO have been presented above.

In all cases it is difficult to determine an as clear and significant widespread pattern as observed in the case of AO/NAO.

Nevertheless, we should be aware of the limitations of the present study. First of all, the data set has been obtained by assimilation of measurements and satellite remote-sensed data into a global model. The imperfections of the model and the assimilation schemes are accordingly bound to influence the computed output. Due to the spatial resolution of  $1/2^\circ$  (lat)  $\times$   $2/3^\circ$  (long) some local effects that change wind speeds such as mountain passes and valleys are not represented. In addition, since the teleconnection indices have time resolution of at least one day, intermittency and other phenomena of higher scale and their effects can only be studied. Regarding our study about the potential electrical energy output by different model turbines, it is important to note that it aims to give only a qualitative impression of the areas with high potential. Of course, these areas should be examined in detail and the optimal wind turbine has to be determined for every location separately. Further studies should also be conducted on AMO taking into account a longer record of WPD data since AMO may be potentially predictable several decades ahead (Knight et al., 2005). Knowing its influence on WPD could help evaluate wind power output years in advance, and therefore further reduce uncertainty about this promising renewable energy resource. Better understanding of the influence of teleconnections on WPD also helps estimating the potential wind power output of future commercial wind farms. For instance, if the period of time considered to estimate their potential is mainly characterized by one phase of a certain teleconnection having an impact on WPD, the actual wind power output in the following ten years could turn out to be overestimated, especially if the phase of the teleconnection changes. Thus, the decision about a future investment based on this period of time could be biased, and result in a non-profitable financing. Similarly, areas of high wind power potential could be underestimated by not taking into account the actual phase of an underlying teleconnection. Our study clearly underlines that the interconnection of the electricity grids over whole Europe should be a priority for the European Union given the potential to balance the teleconnectivity from AO/NAO. A study on the economic feasibility of interconnection of wind farms, and the resulting losses due to the transmission of electrical current, should be conducted. In addition, it would be interesting to study the correlations between teleconnection indices and real wind power that has been harvested by wind farm operators using electricity generation data over all of Europe as it has been done for Spain by Jerez et al. (2013).

### **Acknowledgements**

First of all, I would like to express my sincere thanks to Mr Hervé Le Treut and Prof. Ronald G. Prinn for having given me the opportunity to work for the MIT Joint Program on the Science and Policy of Global Change. In addition, I want to thank Alexandra Cosseron for helping me

preparing this research internship, Charles Fant, Yohannes Gebretsadik and Udaya Bhaskar Gunturu for the help they provided regarding Matlab and the Institute's server system as well as Erwan Monier for the interesting discussions and his suggestions. Last but not least, a huge thank you to Adam Schlosser for his trust through all my research. I am extremely grateful for his useful remarks as well as his friendly and highly motivating nature.

Furthermore, I would like to acknowledge the GMAO and the GES DISC for the dissemination of MERRA.

## 6. REFERENCES

- Ambaum, M. H. P., Hoskins, B. J., Stephenson, D. B., 2001: Arctic Oscillation or North Atlantic Oscillation?. *J. Climate*, 14, 3495-3507.
- Archer, C. L., and Jacobson, M. Z., 2007: Supplying Baseload Power and Reducing Transmission Requirements by Interconnecting Wind Farms. *J. Appl. Meteorol. Clim.*, 46, 1701-1717.
- Atkinson, N., Harman, K., Lynn, M., Schwarz, A., Tindal, A., 2006: Long-Term Wind Speed Trends in Northwestern Europe. Technical Report, 14.
- Baldwin, M. P., and Dunkerton, T. J., 2001: Stratospheric harbingers of anomalous weather regimes. *Science* 294, 581-584.
- Brayshaw, D. J., Troccoli, A., Fordham, R., Methven, J., 2011: The impact of large scale atmospheric circulation patterns on wind power generation and its potential predictability: A case study over the UK Renewable Energy, Volume 36, Issue 8, 2087–2096.
- Brönnimann, S., 2007: Impact of El Niño–Southern Oscillation on European climate. *Rev. Geophys.*, 45, RG3003.
- Cosseron, A., Gunturu, U. B., Schlosser, C. A., 2013, Characterization of the wind power resource in Europe and its intermittency. *Energy Procedia*, 40C, pp. 58-66.
- Deser, C., 2000: On the teleconnectivity of the Arctic oscillation. *Geophys. Res. Lett.*, 27, 779-782.
- EC, European Commission, Energy infrastructure. URL: [http://ec.europa.eu/energy/infrastructure/north\\_south\\_east\\_en.htm](http://ec.europa.eu/energy/infrastructure/north_south_east_en.htm)
- Elliot, D. L., Holladay, C. G., Barchet, W. R., Foote, H. P., Sandusky, W. F., 1987: Wind Energy Resource Atlas of the United States. DOE/CH 10093-4, Solar Energy Research Institute, Golden, Colorado.
- EWEA, 2013: EWEA Annual Report 2012. URL: [http://www.ewea.org/fileadmin/files/library/publications/reports/EWEA\\_Annual\\_Report\\_2012.pdf](http://www.ewea.org/fileadmin/files/library/publications/reports/EWEA_Annual_Report_2012.pdf)
- Fraedrich, K., and Müller, K., 1992: Climate anomalies in Europe associated with ENSO extremes. *Int. J. Climatol.*, 12, 25-31.

- Gasch, R. and Twele, J., 2011: Wind Power Plants. Springer, Berlin, Second Edition, 141 pp.
- Goldenberg, S. B., Landsea, C. W., Mestas-Nuñez, A. M., Gray, W. M., 2001: The recent increase in Atlantic hurricane activity: Causes and implications. *Science*, 293, 474-479.
- Gray, S. T., Graumlich, L. J., Betancourt, J. L., Pederson, G. T., 2004: A tree-ring based reconstruction of the Atlantic multidecadal oscillation since 1567 AD. *Geophys. Res. Lett.*, 31, L12205.
- Gunturu, U. B., and Schlosser, C. A., 2012: Characterization of wind power resource in the United States. *Atmos. Chem. Phys.*, 12, 9687-9702.
- Gustavson, M. R., 1979: Limits to Wind Power Utilization. *Science*, 204(4388), 1317.
- Hennessey J. Jr., 1977: Some Aspects of Wind Power Statistics. *J. Appl. Meteorol.*, 16, 119-128.
- Hurrell, J. W., 1995: Decadal trends in the North Atlantic oscillation: Regional temperatures and precipitation. *Science*, 269, 676-679.
- Hurrell, J. W., Kushnir, Y., Ottersen, G., Visbeck, M. (Eds.), 2003: The North Atlantic Oscillation: Climatic Significance and Environmental Impact. *Geophys. Monogr. Ser.*, Washington DC, vol. 134, 279 pp.
- Hurrell, J. W., and Deser, C., 2009: North Atlantic climate variability: The role of the North Atlantic Oscillation. *Journal of Marine Systems*, Volume 78, Issue 1, 28-41.
- Jaramillo, O. A., and Borja, M. A., 2004: Wind speed analysis in La Ventosa, Mexico: a bimodal probability distribution case *Renewable Energy*. Volume 29, Issue 10, 1613–1630.
- Jerez, S., Trigo, R., Vicente-Serrano, S., Pozo-Vázquez, A., Lorente-Plazas, R., Lorenzo-Lacruz, J., Santos-Alamillos, F., and Montávez, J., 2013: The impact of the North Atlantic Oscillation on the renewable energy resources in south-western Europe. *J. Appl. Meteor. Climatol.*, in press.
- Jolliffe, I. T., 1986: *Principal Component Analysis*. Springer, New York, Second Edition, 290 pp.
- Kerr, R. A., 2000: A North Atlantic climate pacemaker for the centuries. *Science* 288, 1984-1986.
- Kiss, P., and Janosi, I. M., 2008: Limitations of wind power availability over Europe: a conceptual study. *Nonlin. Processes Geophys.*, 15, 803-813.
- Knight, J. R., Allan, R. J., Folland, C. K., Vellinga, M., Mann, M. E., 2005: A signature of persistent natural thermohaline circulation cycles in observed climate. *Geophys. Res. Lett.*, 32, L20708.
- Kushnir, Y., 1994: Interdecadal Variations in North Atlantic Sea Surface Temperature and Associated Atmospheric Conditions. *J. Climate*, 7, 141-157.



- Kutzbach, J. E., 1970: Large-scale features of monthly mean Northern Hemisphere anomaly maps of sea-level pressure. *Mon. Wea. Rev.*, 98, 708-716.
- Landberg, L., Giebel, G., Nielsen, H. A., Nielsen, T., Madsen, H., 2003: Short-term prediction-An overview. *Wind Energy*, 6, 273-280.
- Larsen, X. G., and Mann, J., 2009: Extreme Winds from the NCEP/NCAR Reanalysis Data. *Wind Energ.*, 12, 556-573.
- Lau, N., 1988: Variability of the Observed Midlatitude Storm Tracks in Relation to Low-Frequency Changes in the Circulation Pattern. *J. Atmos. Sci.*, 45, 2718-2743.
- Lorenz, E. N., 1950: Seasonal and irregular variations of the Northern Hemisphere sea-level pressure profile. *J. Meteor.*, 8, 52-59.
- Meneveau, C., and Meyers, J., 2010: Optimization of Turbine Spacing in the Fully Developed Wind Turbine Array Boundary Layer. *Bulletin of the American Physical Society*, 55.
- Morrissey, M. L., Cook, W. E., Greene, J. S., 2010: An Improved Method for Estimating the Wind Power Density Distribution Function. *J. Atmos. Oceanic Technol.*, 27, 1153–1164.
- NOAA, National Oceanic and Atmospheric Administration, Climate Prediction Center.  
URL: [http://www.cpc.ncep.noaa.gov/products/precip/CWlink/daily\\_ao\\_index/teleconnections.html](http://www.cpc.ncep.noaa.gov/products/precip/CWlink/daily_ao_index/teleconnections.html)
- Philander, S. G., 1989: *El Niño, La Nina, and the Southern Oscillation*. Elsevier, New York, Vol. 46.
- Pirazzoli, P. A., Tomasin, A., Ullmann, A., 2010: Recent changes in measured wind in the NE Atlantic and variability of correlation with NAO. *Ann. Geophys.*, 28, 1923-1934.
- Pryor, S. C., Barthelmie, R. J., Schoof, J. T., 2006: Inter-annual variability of wind indices across Europe. *Wind Energ.*, 9, 27-38.
- Rienecker, M. M., Suarez, M. J., Gelaro, R., Todling, R., Bacmeister, J., Liu, E., Bosilovich, M. G., Schubert, S. D., Takacs, L., Kim, G., Bloom, S., Chen, J., Collins, D., Conaty, A., da Silva, A., Gu, W., Joiner, J., Koster, R. D., Lucchesi, R., Molod, A., Owens, T., Pawson, S., Pegion, P., Redder, C. R., Reichle, R., Robertson, F. R., Ruddick, A. G., Sienkiewicz, M., and Woollen, J., 2011: MERRA – NASA's Modern-Era Retrospective Analysis for Research and Applications. *J. Climate*, 24.
- Rogers, J. C., 1997: North Atlantic Storm Track Variability and Its Association to the North Atlantic Oscillation and Climate Variability of Northern Europe. *J. Climate*, 10, 1635-1647.
- Ropelewski, C. F., and Halpert, M. S., 1987: Global and regional scale precipitation patterns associated with the El Niño/Southern Oscillation (ENSO). *Mon. Weather Rev.*, 115, 1606-1626.

- Schlesinger, M. E., and Ramankutty, N., 1994: An oscillation in the global climate system of period 65-70 years. *Nature*, 367, 723-726.
- Stull, R., 1988: *An Introduction to Boundary Layer Meteorology*. Springer, Boston, 13.
- Sutton, R. T., and Hodson, D. L. R., 2005: Atlantic Ocean forcing of North American and European summer climate. *Science* 309, 115-118.
- Thompson, D. W. J., and Wallace, J. M., 1998: The Arctic oscillation signature in wintertime geopotential height and temperature fields. *Geophys. Res. Lett.*, 25, 1297-1300.
- Torres, J. L., García, M., De Blas, M., De Francisco, A., 2005: Forecast of hourly average wind speed with ARMA models in Navarre (Spain). *Sol. Energy*, 79, 65-77.
- Ulbrich, U., Christoph, M., 1999: A shift of the NAO and increasing storm track activity over Europe due to anthropogenic greenhouse gas forcing. *Climate Dynamics*, Volume 15, Issue 7, 551-559.
- Van Loon, H., and Rogers, J. C., 1978: The seesaw in winter temperatures between Greenland and northern Europe. Part I: Winter, *Mon. Weath. Rev.*, 10, 365-380.
- VESTAS, 2013: Product brochures: 2 MW Platform (p. 8-9), Vestas V90-3.0MW (p. 11-11), 3 MW Platform (p.10-11). Vestas. URL: <http://www.vestas.com/en/media/brochures.aspx>
- Visbeck, M., Cullen, H., Krahlmann, G., Naik, N., 1998: An ocean model's response to north Atlantic Oscillation-like wind forcing. *Geophys. Res. Lett.*, 25, 4521-4524.
- Von Storch, H., Zwiers F.W., 2002: *Statistical Analysis in climate Research*. Cambridge University Press, Cambridge, 99-118.
- Wallace, J. M., and Gutzler, D. S., 1981: Teleconnections in the geopotential height field during the Northern Hemisphere winter. *Mon. Wea. Rev.*, 109, 784-812.
- Watson, S. J., Landberg, L., Halliday, J. A., 1994: Application of wind speed forecasting to the integration of wind energy into a large scale power system. *IEE Proc. Gener. Transm. Distrib.*, 141, 357-362.
- Woollings, T., 2010: Dynamical influences on European climate: An uncertain future. *Philos. Trans. Roy. Soc. London*, 368A, 3733-3756.

## 7. APPENDIX

### 7.1 Acronyms

ADAS : Atmospheric Data Assimilation System

AMO : Atlantic Multidecadal Oscillation

AO : Arctic Oscillation

EA: East Atlantic teleconnection

ECMWF : European Center for Medium-Range Weather Forecasts

EEA : European Environment Agency

ENSO : El Niño Southern Oscillation

EOF: Empirical Orthogonal Function

ERA : ECMWF Reanalysis

ERA-40 : A 45-year ERA from September 1957 to August 2002

FSL : Forecast Systems Laboratory

GDF : Great Dunfell

GMAO : Global Modeling and Assimilation Office

GSI : Grid-point Statistical Interpolation

MERRA : Modern-Era Retrospective Analysis for Research and Applications

NAO : North Atlantic Oscillation

NASA : National Aeronautics and Space Administration

NCAR : National Center for Atmospheric Research

NCDC : National Climatic Data Center

NCEP : National Center for Environmental Prediction

NOAA : National Oceanic and Atmospheric Administration

PC : Principal Component

PDF : Probability Density Function

PNA : Pacific North American Pattern

SLP : Sea Level Pressure

SST : Sea Surface Temperature

STO : Stornoway

UK: United Kingdom

WPD : Wind Power Density

WS : Wind Speed

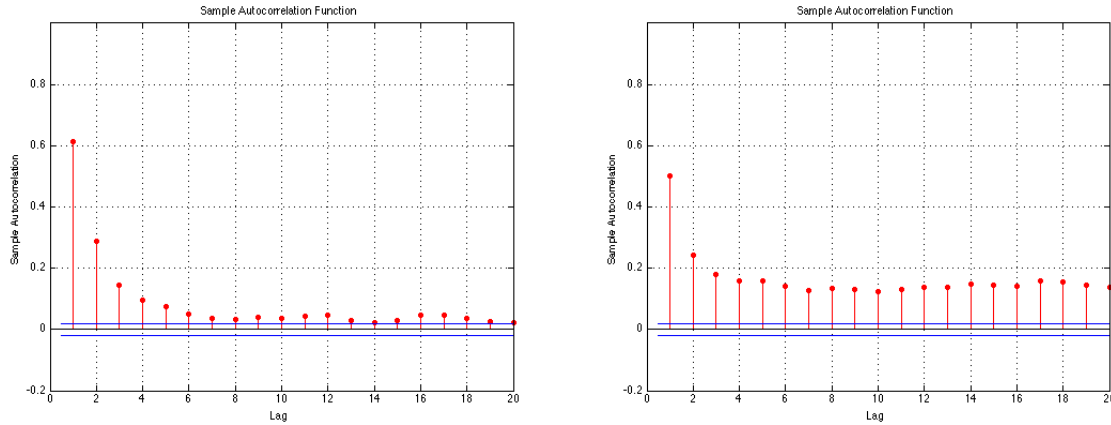


**Figure 30.** Autocorrelation of 31-year cold season WPD data for two grid points in order to determine the number of independent data points.

## 7.2 Determination of Statistical Significance

As we calculated the correlation coefficient  $r$  in different studies above, we needed to determine the likelihood that it only occurred by chance. In order to calculate the respective critical absolute values for  $r$  we first had to estimate the degree of freedoms present in the data set used. These are varying with changing time periods of the moving averages that are applied. We estimated these degrees of freedom or independent data points by autocorrelation. Therefore we calculated the mean and the median lag over all grid points at which the slope of the sample autocorrelation turns positive for the first time and chose the higher one of both since we are looking for an underestimate for the degrees of freedom. For instance, we obtained a mean lag of 6,9 for the daily non averaged WPD data over 31 years of the cold season, and thus  $\frac{4689}{6,9} = 675$  independent data points. That is completely consistent with what we have expected since weather conditions are changing about all 3-6 days. Now we were able to calculate the critical statistical value at different significance levels  $\alpha$  (1% and 5%) in Excel. A significance level of 1% means that there is a 1% risk of error that the null hypothesis is rejected when it is true. **Figure 30** shows two examples of autocorrelation plots for two different grid points. Naturally, we choose the lower degree of freedom of the two time series in question to estimate the critical  $r$ .

In our linear regression studies we used a different method to determine the critical absolute values for  $R^2$ , called slope-test. After preparing our data by averaging out the dependent data points (that have been determined as described above), we state our Null hypothesis that the slope of the regression line is zero. Then we choose a significance level and conduct a t-test to determine if the slope of the regression line differs significantly from 0. Since the Matlab-function used to calculate  $R^2$  directly provides the necessary p values we only need to test if  $p < \alpha$  at each grid point. If yes, the result at the respective grid point is statistically significant at a significance level of  $\alpha$ .

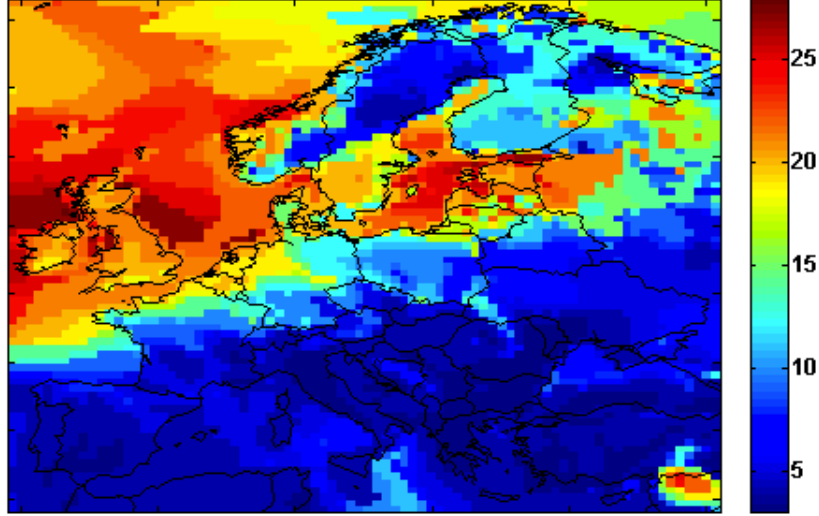


**Figure 31.** Geographical variation of the lag in autocorrelation of the WPD sample for a strong positive AO phase. We obtain a overall mean of 5,8 and a median of 5,0 whereas the lag over land is rather between 3 and 4 days.

In order to assess the significance of the impact of a change in phase (e.g. from „low“ to „high“) of a certain teleconnection we applied a two-tailed t-tests for the null hypothesis of equal means. Therefore we use formula (19) according to von Storch and Zwiers (2002). Let  $n_{high}$  and  $n_{low}$  denote the degrees of freedom of the sample of WPD events  $X_{high}$  and  $X_{low}$  during a high and a low phase respectively and  $\mu_{high}$  as well as  $\mu_{low}$  the mean of each sample.

$$t = \frac{\mu_{high} - \mu_{low}}{\sqrt{\left(\frac{1}{n_{high}} + \frac{1}{n_{low}}\right) \sqrt{\frac{(n_{high}-1)Var(X_{high}) + (n_{low}-1)Var(X_{low})}{n_{high} + n_{low} - 2}}}} \quad (11)$$

The critical t-values are extracted from a table for a two tailed distribution taking into account the respective degree of freedom of our data and a level of significance  $\alpha$  that has been carefully chosen in every case. These critical values are compared to the t-value obtained at every gridpoint and a result is accepted as significant at a certain level  $\alpha$  if  $|t| > t_{crit}$ .

Again, it is important to note that we are underestimating the confidence level in all our assumptions. For instance, WPD is varying much more over land than over sea as can be seen in **Figure 31**. Thus, we have a higher number of degrees of freedom over land. As a result, by calculating the mean or the median lag over every gridpoint we are underestimating the number of independent data points over land which is the region we are most interested in.

## REPORT SERIES of the MIT Joint Program on the Science and Policy of Global Change

FOR THE COMPLETE LIST OF JOINT PROGRAM REPORTS:  
<http://globalchange.mit.edu/pubs/all-reports.php>

205. **Quantifying the Likelihood of Regional Climate Change: A Hybridized Approach** Schlosser et al. October 2011
206. **Process Modeling of Global Soil Nitrous Oxide Emissions** Saikawa et al. October 2011
207. **The Influence of Shale Gas on U.S. Energy and Environmental Policy** Jacoby et al. November 2011
208. **Influence of Air Quality Model Resolution on Uncertainty Associated with Health Impacts** Thompson and Selin December 2011
209. **Characterization of Wind Power Resource in the United States and its Intermittency** Gunturu and Schlosser December 2011
210. **Potential Direct and Indirect Effects of Global Cellulosic Biofuel Production on Greenhouse Gas Fluxes from Future Land-use Change** Kicklighter et al. March 2012
211. **Emissions Pricing to Stabilize Global Climate** Bosetti et al. March 2012
212. **Effects of Nitrogen Limitation on Hydrological Processes in CLM4-CN** Lee & Felzer March 2012
213. **City-Size Distribution as a Function of Socio-economic Conditions: An Eclectic Approach to Down-scaling Global Population** Nam & Reilly March 2012
214. **CliCrop: a Crop Water-Stress and Irrigation Demand Model for an Integrated Global Assessment Modeling Approach** Fant et al. April 2012
215. **The Role of China in Mitigating Climate Change** Paltsev et al. April 2012
216. **Applying Engineering and Fleet Detail to Represent Passenger Vehicle Transport in a Computable General Equilibrium Model** Karplus et al. April 2012
217. **Combining a New Vehicle Fuel Economy Standard with a Cap-and-Trade Policy: Energy and Economic Impact in the United States** Karplus et al. April 2012
218. **Permafrost, Lakes, and Climate-Warming Methane Feedback: What is the Worst We Can Expect?** Gao et al. May 2012
219. **Valuing Climate Impacts in Integrated Assessment Models: The MIT IGSM** Reilly et al. May 2012
220. **Leakage from Sub-national Climate Initiatives: The Case of California** Caron et al. May 2012
221. **Green Growth and the Efficient Use of Natural Resources** Reilly June 2012
222. **Modeling Water Withdrawal and Consumption for Electricity Generation in the United States** Strzepek et al. June 2012
223. **An Integrated Assessment Framework for Uncertainty Studies in Global and Regional Climate Change: The MIT IGSM** Monier et al. June 2012
224. **Cap-and-Trade Climate Policies with Price-Regulated Industries: How Costly are Free Allowances?** Lanz and Rausch July 2012.
225. **Distributional and Efficiency Impacts of Clean and Renewable Energy Standards for Electricity** Rausch and Mowers July 2012.
226. **The Economic, Energy, and GHG Emissions Impacts of Proposed 2017–2025 Vehicle Fuel Economy Standards in the United States** Karplus and Paltsev July 2012
227. **Impacts of Land-Use and Biofuels Policy on Climate: Temperature and Localized Impacts** Hallgren et al. August 2012
228. **Carbon Tax Revenue and the Budget Deficit: A Win-Win Solution?** Sebastian Rausch and John Reilly August 2012
229. **CLM-AG: An Agriculture Module for the Community Land Model version 3.5** Gueneau et al. September 2012
230. **Quantifying Regional Economic Impacts of CO<sub>2</sub> Intensity Targets in China** Zhang et al. September 2012
231. **The Future Energy and GHG Emissions Impact of Alternative Personal Transportation Pathways in China** Kishimoto et al. September 2012
232. **Will Economic Restructuring in China Reduce Trade-Embodied CO<sub>2</sub> Emissions?** Qi et al. October 2012
233. **Climate Co-benefits of Tighter SO<sub>2</sub> and NO<sub>x</sub> Regulations in China** Nam et al. October 2012
234. **Shale Gas Production: Potential versus Actual GHG Emissions** O'Sullivan and Paltsev November 2012
235. **Non-Nuclear, Low-Carbon, or Both? The Case of Taiwan** Chen December 2012
236. **Modeling Water Resource Systems under Climate Change: IGSM-WRS** Strzepek et al. December 2012
237. **Analyzing the Regional Impact of a Fossil Energy Cap in China** Zhang et al. January 2013
238. **Market Cost of Renewable Jet Fuel Adoption in the United States** Winchester et al. January 2013
239. **Analysis of U.S. Water Resources under Climate Change** Blanc et al. February 2013
240. **Protection of Coastal Infrastructure under Rising Flood Risk** Lickley et al. March 2013
241. **Consumption-Based Adjustment of China's Emissions-Intensity Targets: An Analysis of its Potential Economic Effects** Springmann et al. March 2013
242. **The Energy and CO<sub>2</sub> Emissions Impact of Renewable Energy Development in China** Zhang et al. April 2013
243. **Integrated Economic and Climate Projections for Impact Assessment** Paltsev et al. May 2013
244. **A Framework for Modeling Uncertainty in Regional Climate Change** Monier et al. May 2013
245. **Climate Change Impacts on Extreme Events in the United States: An Uncertainty Analysis** Monier and Gao May 2013
246. **Probabilistic Projections of 21<sup>st</sup> Century Climate Change over Northern Eurasia** Monier et al. July 2013
247. **What GHG Concentration Targets are Reachable in this Century?** Paltsev et al. July 2013
248. **The Energy and Economic Impacts of Expanding International Emissions Trading** Qi et al. August 2013
249. **Limited Sectoral Trading between the EU ETS and China** Gavard et al. August 2013
250. **The Association of Large-Scale Climate Variability and Teleconnections on Wind Resource over Europe and its Intermittency** Kriesche and Schlosser September 2013